The *E. coli* DnaX clamp loader sharply bends DNA to load β-clamp at nicks and small gaps

Fengwei Zheng[1,#], Nina Y. Yao[2,#], Roxana E. Georgescu[2], Meinan Lyu[1],
Michael E. O'Donnell[2,*], and Huilin Li[1,3,*]
[1] Department of Structural Biology, Van Andel Institute, Grand Rapids, Michigan, USA.
[2] DNA Replication Laboratory and Howard Hughes Medical Institute, The Rockefeller University, New York, New York, USA
[3] Lead contact
[#] These authors contributed equally to this work.

[*] Correspondence should be addressed to M.E.O (odonnel@rockefeller.edu) or H.L (Huilin.Li@vai.org)

In brief: Zheng et al. show that the bacterial clamp loader DnaX-complex uses a DNA-bending mechanism—rather than DNA unwinding—to load the β-clamp at nicks and small gaps, revealing a clamp-loading strategy distinct from eukaryotic RFC and relevant to DNA damage repair.

Highlights

- The bacterial DnaX clamp loader lacks a stable shoulder DNA-binding site
- Unlike eukaryotic RFC, DnaX does not unwind DNA at nicks and small gaps
- The *E. coli* β-clamp contains a conserved external DNA-binding site absent in PCNA
- Sharp DNA bending enables β-clamp loading at nicks and small ssDNA gaps

Abstract. DNA sliding clamps are essential for processive DNA synthesis in all domains of life and are loaded by ATP-dependent clamp loaders that recognize recessed 3′ ends. How clamp loaders function at nicks and small ssDNA gaps—common intermediates during DNA repair—remains incompletely understood. Here, we show that the bacterial *Escherichia coli* DnaX clamp loader employs a fundamentally different mechanism from its eukaryotic counterpart. Whereas eukaryotic RFC unwinds DNA at the recessed 3′ end and stabilizes the 5′-dsDNA at a dedicated shoulder site, the bacterial DnaX-complex neither unwinds DNA nor stably binds the 5′-dsDNA in vitro. Instead, cryo-EM structures reveal that the β-clamp itself contains a conserved external DNA-binding site that enables sharp bending of gapped DNA by ~150°, promoting insertion of the 3′-dsDNA into the clamp. This DNA-bending mechanism allows efficient β-clamp loading at nicks and small gaps and reveals a distinct bacterial strategy for clamp loading. Because small DNA gaps are frequently associated with DNA damage, clamps loaded at these sites are likely important for DNA repair.

Introduction

In all cell types—bacteria, archaea and eukaryotes—the DNA replication machinery utilizes ring-shaped clamps that encircle duplex DNA and tether replicative DNA polymerases (Pols) to DNA, enabling rapid and highly processive synthesis[1-4]. This function is readily apparent in the *Escherichia coli* (*E. coli*) Pol III replication system, in which circular clamps were first discovered[1]. In the absence of a clamp, *E. coli* Pol III core synthesizes DNA at only ~1 nucleotide (nt) per second; upon engagement with its β-clamp, Pol III synthesizes DNA at >500 nt per second with extremely high processivity (>5 kb)[1]. Because circular sliding clamps cannot self-assemble onto DNA, they require an ATP-driven clamp loader that recognizes a DNA 3′-recessed end and loads the clamp onto it[3,4].

In *E. coli*, the β-clamp is a homodimer, with each protomer containing three domains of identical fold, giving the clamp pseudo–six-fold symmetry. The eukaryotic equivalent, PCNA, is a homotrimer in which each subunit contains two domains of the same fold, also forming a pseudo–six-fold symmetric ring[2,5,6] (**Figure 1A**). The *E. coli* clamp loader motor consists of one δ subunit, one δ′ subunit, and three *dnaX*-encoded subunits[7,8]. The *dnaX* gene produces two isoforms: a full-length τ subunit and a shorter γ subunit generated by translational frameshifting[8] (**Figure 1B**). In this study, we refer to this pentameric motor assembly as the DnaX-complex. The bacterial clamp loader also contains two small accessory subunits, χ and ψ, which are not required for clamp loading per se[8]. The full seven-subunit assembly is referred to here as the DnaX-holo-complex. The eukaryotic counterpart of the DnaX-complex is the heteropentameric Replication Factor C (RFC) clamp loader[4,9].

Crystal structures of both the DnaX-complex and RFC revealed that these clamp loaders adopt similar overall architectures[7,10]. Each forms a spiral-shaped pentamer with a central chamber that accommodates dsDNA and features a prominent gap between δ and δ′ subunits through which DNA enters the chamber. The sliding clamp is positioned directly beneath this chamber, explaining how clamp loaders guide DNA into the open clamp[3]. In both systems, ATP-binding sites are located at subunit interfaces, a hallmark of AAA+ ATPases, allowing coordinated inter-subunit communication during the clamp loading cycle[3,11].

Clamp loading at large ssDNA gaps, such as those between Okazaki fragments, is well understood for both eukaryotic RFC[12-15] and the bacterial DnaX-complex[16,17]. In both cases, the clamp remains closed in solution until binding by the clamp loader induces gate opening[18]. A notable difference is that DnaX-complex opens the β-clamp in a counterclockwise direction, whereas RFC opens PCNA clockwise[16], consistent with earlier biochemical studies demonstrating opposite directionality in bacterial and eukaryotic clamp opening[19,20]. Following clamp opening, the DNA 3′-recessed end is recognized by the clamp loader chamber, dsDNA enters the clamp, and the clamp subsequently closes around the DNA.

These steps require ATP binding but not ATP hydrolysis[16,17,21]. ATP hydrolysis then triggers dissociation of the clamp loader, completing the loading reaction[22-24].

Biochemical studies have shown that both the bacterial and eukaryotic clamp loaders can load clamps at a nick or small ssDNA gaps (<6 nt), a process relevant to DNA repair. Clamp loading at such sites is more challenging and remains an active area of investigation. Recent structural studies demonstrated that eukaryotic RFC unwinds DNA from the 3′-recessed end to widen small gaps and revealed an external "shoulder" DNA-binding site that stabilizes the dsDNA segment at the 5′-recessed end (hereafter 5′-dsDNA)[12-15]. This shoulder site is formed by the unique Rfc1 BRCT domain together with the Rfc1 AAA+ domain and allows RFC to simultaneously bind both the 3′- and 5′-dsDNA segments[25-27] (**Figure 1A**). The ability of RFC to function at small gaps has been shown to correlate with DNA repair[12-15].

How the bacterial DnaX-complex loads clamps onto nicked or small-gapped DNA has not previously been visualized. Consequently, it has remained unclear whether the bacterial clamp loader possesses a functional shoulder DNA-binding site or whether it unwinds DNA in a manner analogous to eukaryotic RFC (**Figure 1A**). To address these questions, we used cryo-EM to determine structures of the DnaX-complex bound to the β-clamp and DNA substrates containing 1- or 10-nt gaps. We captured a total of 13 clamp loading intermediates (**Supplemental video 1**) and found that, in contrast to RFC, the bacterial DnaX-complex neither unwinds DNA nor stably binds the 5′-dsDNA at the shoulder site under our in vitro conditions. Instead, we uncover a distinct clamp loading mechanism in which the β-clamp utilizes an external DNA-binding site to enable sharp DNA bending, allowing clamp loading at nicks and small gaps.

RESULTS

1. Cryo-EM of bacterial DnaX-complex with β-clamp and 1-nt gapped DNA

Previous studies of the eukaryotic RFC demonstrated that it can unwind up to 6 bp at a DNA nick to generate a sufficiently long ssDNA gap for clamp loading[14,15]. Although earlier biochemical studies showed that the *E. coli* DnaX-complex can load clamps onto nicked DNA[1], whether the bacterial loader unwinds DNA in a manner analogous to eukaryotic RFC has remained unclear (**Figure 1A**).

The *E. coli dnaX* gene encodes two isoforms, the full-length τ subunit and a C-terminally truncated γ subunit. As a result, the seven-subunit bacterial loader complex can exist in two forms, one containing three τ subunits ($\tau_3\delta\delta'$) and another containing three γ subunits ($\gamma_3\delta\delta'$) (**Figure 1B**). In this study, we used the full-length τ-containing complex (τ_3, hereafter referred to as "τ-complex") for cryo-EM analysis to capture structural features of the τ C-terminal region that was absent in previous crystal structures[7,28]. For subsequent biochemical assays, we used the γ-containing complex (γ_3, hereafter referred to as

107 the“γ-complex”), which has equivalent clamp loading activity and has been extensively characterized in
108 prior biochemical studies[29,30].
109
110 To investigate how the DnaX-complex loads the β-clamp onto small gaps (<6 nt) and whether it unwinds
111 DNA in this context, we assembled in vitro clamp loading intermediates by mixing purified τ-complex, β-
112 clamp, and a 1-nt gapped DNA substrate (**Figure 1C**) at a molar ratio of 1:1.3:1.5 in the presence of 5
113 mM Mg^{2+} and 0.5 mM ATPγS, a slowly hydrolyzable ATP analog[31]. Cryo-EM grids were prepared from
114 this mixture, and data were collected and processed as described below. Two major loading states were
115 resolved, corresponding to early and late stages of the clamp loading reactions (**Figure S1**, **Table S1**).
116
117 **2. DnaX-complex does not possess a stable shoulder binding site for 5′-dsDNA**
118 In the first major loading state, the β-clamp is open, but the 3′-dsDNA has yet entered the clamp. The
119 DNA 3′-recessed end resides inside the loader chamber, oriented towards the δ-subunit residue Y316.
120 However, the 3′-dsDNA tilts outwards by ~52° away from the β-clamp and does not enter the clamp
121 interior, but instead rests on the outer surface of the open clamp. We therefore refer to this conformation
122 as the “DNA gap recognition” state (**Figure 1D**). This disposition of the 3′-dsDNA is unprecedented. In all
123 structurally visualized clamp loading intermediates—whether bacterial or eukaryotic—the 3′-dsDNA is
124 either unresolved or has fully entered the clamp chamber.
125
126 Density corresponding to the 5′-dsDNA was weak and variable near the shoulder region of the DnaX-
127 complex (**Figure 1D**). Further 3D classification resolved three conformers at resolutions ranging from
128 3.14 to 2.71 Å, differing primarily in the extent of 5′-dsDNA ordering (**Figure S1**). In conformer 1,
129 approximately 9 bp of the 5′-dsDNA are ordered; in conformer 2, only 5 bp are ordered; and in conformer
130 3, the 5′-dsDNA is completely disordered. Notably, conformer 1 accounts for only ~6% of particles in this
131 state, indicating that the DnaX-complex does not stably bind the 5′-dsDNA at the shoulder site.
132 Moreover, from conformer 1 to conformer 3, the 3′-dsDNA moves incrementally toward clamp chamber,
133 as indicated by the cyan arrow in **Figure 1D**.
134
135 In this DNA gap recognition state, the β-clamp gate is opened by ~28 Å (**Figure 1E**), which is wider than
136 the 20 Å opening previously observed for the DnaX-complex bound to a tailed DNA substrate[16]. This
137 wider opening may be stabilized by interactions with the blunt end of the 3′-dsDNA.
138
139 **3. DnaX-complex sharply bends DNA for loading β-clamp onto 1-nt gapped DNA**
140 In the second major loading state, the 3′-dsDNA has fully entered the chambers of both the DnaX-
141 complex and the β-clamp, representing a post–DNA–entry state. Further classification of this state

142 yielded two conformers at resolutions of 2.72 Å and 3.12 Å, respectively, which differ in β-clamp gate
143 width and DNA positioning (**Figures 2A, S1**).
144
145 In state 2 conformer 1, the β-clamp gate narrows from the 28 Å opening observed in the DNA gap
146 recognition state to 24 Å. In this conformer, the 5′-dsDNA bends sharply downward by ~150° and binds
147 to the outer surface of the β-clamp at the site previously occupied by the 3′-dsDNA in the DNA gap
148 recognition state (**Figure 2A**–**C**). In state 2 conformer 2, the 3′-dsDNA enters the β-clamp further, the 5′-
149 dsDNA dissociates from the clamp and became less sharply bent (~137°), and the β-clamp gate narrows
150 further to ~17 Å (**Figure 2B**–**C**).
151
152 Together, these two conformers suggest a clamp-loading mechanism in which sharp bending of the 5′-
153 dsDNA promotes insertion of the 3′-dsDNA into the β-clamp chamber, followed by progressive clamp
154 closure.
155
156 **4. A unique basic patch on β-clamp is utilized in clamp loading onto small gapped DNA**
157 The repeated binding of 3′-dsDNA in the first loading state and 5′-dsDNA in the second loading state
158 binding to the outer surface of the open β-clamp led us to identify a basic patch on the β-clamp surface.
159 This patch is formed by three positively charged residues—R96, R103, and R105—which lie within ~3.5
160 Å of the DNA (**Figure 2D**). Structure-based sequence alignment of bacterial β-clamps, spanning
161 sequence identities 29% to 96%, revealed strong conservation of those three arginine residues (**Figure**
162 **S2A–B**). In contrast, the corresponding region in yeast and human PCNA is acidic (**Figure 2E**).
163
164 To examine the functional importance of this basic patch, we incorporated an N-terminal peptide ^{32}P-
165 labeling motif in wild-type β-clamp (β-clamp$_{WT}$) and generated two mutants by substituting the arginine
166 residues with either alanine (β-clamp$_{Mut1}$) or aspartic acid (β-clamp$_{Mut2}$). We then quantified clamp loading
167 efficiency onto pUC19 plasmid DNA containing a 6-nt gap using a gel-filtration–based assay[19,32-34] (see
168 **STAR METHODS**). Consistent with previous studies indicating that gaps of ≥6 nt are optimal for clamp
169 loading[13-15,31], both β-clamp$_{Mut1}$ and β-clamp$_{Mut2}$ exhibited markedly reduced loading efficiencies,
170 achieving ~35% and ~25%, respectively, of the loading observed with β-clamp$_{WT}$ (**Figure 2F**). Mass
171 photometry confirmed that both mutants remained dimeric in solution (**Figure S2C**),
172
173 We further examined the ability of these β-clamp basic patch mutants to assemble with the DnaX-
174 complex and 1-nt gapped DNA by cryo-EM. 2D classification and 3D reconstruction revealed that, in
175 contrast to wild-type β-clamp, the mutant clamps failed to form complexes in which DNA binds directly to
176 β-clamp surface (**Figure S3A-B**). Together, these results demonstrate a functional role for the conserved
177 β-clamp basic patch in DNA binding and clamp loading at small gaps.

178
179 In addition, we note that a recent cryo-EM study by Landeck et al. reported that, in the absence of DNA,
180 β-clamp domain I—which harbors the basic patch—is disordered[17]. In a comparable state observed here
181 ($RMSD_{C\alpha}$ 0.9 Å), binding of DNA stabilizes this domain, indicating that DNA engagement at the basic
182 patch contributes to the ordering of β-clamp domain I (**Figure S3C**).
183
184 **5. Y316 recognizes but does not separate the DNA 3′ end**
185 The overall architectures of the three conformers in the first loading state and the two conformers in the
186 second loading state are highly similar. Superimposition of the first four conformers onto state 2
187 conformer 2 yields $RMSD_{C\alpha}$ values ranging from 0.8 to 1.0 Å, indicating that the primary structural
188 differences among these intermediates reside in the DNA rather than in the protein components (**Figures**
189 **1C and 2A**).
190
191 Closer examination of residue Y316 of the δ-subunit, previously termed a "separation pin" [28], revealed its
192 role in recognizing—but not unwinding—the DNA 3′ end. In the first loading state, before the 3′-dsDNA
193 enters the loader chamber, Y316 is only partially ordered. From conformer 1 to conformer 3, the distance
194 between the aromatic ring of Y316 and the DNA 3′-junction (i.e., last base of primer 1, G20) decreases
195 from 12.0 Å to 11.4 Å and then to 9.9 Å (**Figure S4**, left). Concurrently, the local cryo-EM density for
196 Y316 becomes progressively stronger, consistent with increasing stabilization of this residue.
197
198 In the second loading state, after the 3'-dsDNA has entered the chamber, Y316 becomes fully ordered
199 and adopts a conformation that mimics a DNA base, stacking against the terminal base of the primer 3'
200 end. In this state, the distance between Y316 and the DNA 3' end is further reduced to 3.5 Å and 3.1 Å in
201 conformers 1 and 2, respectively (**Figure S4**, right). Across all five conformers, we did not observe
202 separation or unwinding of the DNA strands at the 3′ end.
203
204 This absence of DNA unwinding contrasts with observations in eukaryotic RFC clamp loaders, in which
205 the analogous residue can unwind up to 6 bp at the DNA 3′ end[13-15,35]. Taken together, these findings
206 indicate that, rather than functioning as a strand-separation element, Y316 promotes recognition and
207 positioning of DNA 3' end during gap sensing and clamp loading (**Figure S4**).
208
209 **6. The efficiency with which the DnaX-complex loads the β-clamp onto DNA with nicks or small**
210 **gaps**
211 To test the hypothesis that the *E. coli* DnaX-complex employs a distinct strategy to load the β-clamp onto
212 DNA containing nick or small gaps (<6 nt), we compared the clamp loading activities of the wild-type
213 clamp loader ($\gamma\text{-complex}_{WT}$) and a separation-pin mutant bearing the Y316A substitution ($\gamma\text{-complex}_{Mut}$).

214 Clamp loading was assayed using pUC19 plasmid DNA substrate containing either a nick or gaps of
215 defined sizes (**Figure 3A**, see **Methods**).
216
217 For the wild-type clamp loader, the loading efficiency of β-clamp$_{WT}$ onto nicked and 1-nt gapped DNA
218 was approximately half of that observed for DNA substrates containing gaps of 2 nt or larger. In contrast,
219 the γ-complex$_{Mut}$ exhibited a pronounced deficiency in loading the β-clamp onto nicked DNA as well as
220 DNA substrates containing 1-nt and 2-nt gaps (**Figure 3A**, upper). However, loading efficiency by the γ-
221 complex$_{Mut}$ increased progressively with gap size, reaching ~85% and ~90% of wild-type level on DNA
222 substrates containing 4-nt and 6-nt gaps, respectively, and becoming indistinguishable from wild-type on
223 an 8-nt gapped DNA substrate (**Figure 3A**, lower).
224
225 To further correlate these biochemical results with structural observations, we performed cryo-EM
226 analysis of β-clamp loading onto 1-nt gapped DNA using γ-complex$_{Mut}$. Consistent with the loading assay
227 results, we were able to capture only the clamp–clamp loader complex without bound DNA (**Figure S3**).
228 Together, these biochemical and structural data are mutually consistent and strongly support the clamp
229 loading model proposed in **Figure 3B**.
230
231 For loading of PCNA onto small-gapped DNA, the eukaryotic RFC clamp loader unwinds DNA from the
232 3′ end to widen the gap and stabilizes both the 3′- and 5′-dsDNA segments. In contrast, the bacterial
233 DnaX-complex neither unwinds DNA nor stably binds the 5′-dsDNA at a shoulder site under our in vitro
234 conditions. Instead, it loads the β-clamp onto DNA substrates containing gaps smaller than 6 nt by
235 sharply bending the 5′-dsDNA by up to ~150°, whereas RFC induces substantially less 5′-dsDNA
236 bending (~75°)[12-14]. To our knowledge, such an extent of 5′-dsDNA bending during clamp loading has not
237 been previously observed (**Figure 3B; Supplemental Video 2**).
238
239 **7. Cryo-EM of β-clamp loading intermediates with a 10-nt gapped DNA**
240 Using the 1-nt gapped DNA substrate, we established that the *E. coli* DnaX-complex does not unwind the
241 DNA 3′ end, in contrast to its eukaryotic counterpart, and that binding of the 5′-dsDNA at the shoulder
242 site is transient. One possible explanation for these observations is that the extremely short gap
243 physically constrains the DNA such that, when the 3′-dsDNA enters the loader chamber, the 5′-dsDNA is
244 forced away from the shoulder. Alternatively, the bacterial clamp loader may simply lack a functional
245 shoulder DNA-binding site. In addition, the previously unrecognized DNA-binding interaction with the β-
246 clamp basic patch could, in principle, be specific to very short gaps. To distinguish between these
247 possibilities, we performed cryo-EM analysis of β-clamp loading intermediates using a DNA substrate
248 containing a 10-nt gap, which is sufficient long to allow independent positioning of the 3′- and 5′-dsDNA
249 segments (**Figure 4A-B)**.

Cryo-EM image processing yielded eight 3D cryo-EM maps at resolutions ranging from 2.95 to 2.53 Å, corresponding to eight distinct clamp-loading intermediates (**Figure S5, Tables S1** and **S2**). Although the full-length τ-containing DnaX-holo-complex was used for these structural studies, none of the resulting maps resolved density for the C-terminal domains of the three τ subunits, consistent with previous reports[16,17]. Accordingly, the atomic models built for these intermediates include only the γ-region, and the pentameric assembly is referred to here as the DnaX-complex.

Interestingly, all eight maps contained peripheral, low-resolution density visible at lower display thresholds (**Figure S5**), consistent with the presence of the χψ heterodimer. Previous crystallographic and solution studies demonstrated that χψ associates flexibly with the collar domain of the DnaX-complex and can interact with single-stranded DNA–binding protein (SSB)[16,28,36,37]. However, the precise mode of χψ association with the clamp loader has remained unclear.

By applying a focused mask and extensive 3D classification, we obtained a 5.5-Å map corresponding to the χψ heterodimer and merged this density with the first clamp-loading intermediate captured here. The χψ density fits well with the previously reported crystal structure and binds the collar domain of the clamp loader via the ψ subunit. This composite map provides the first overall view of the χψ heterodimer assembled within the DnaX-holo-complex during β-clamp loading.

In the earliest loading intermediate with the 10-nt gapped DNA, the 5′-dsDNA is not resolved, suggesting that it remains flexible outside the clamp–clamp loader complex. The DNA 3′-recessed end is positioned ~3.5 Å from Y316 but is not unwound, and the 3′-dsDNA binds to the outer surface of the open β-clamp via the basic patch, closely resembling the DNA gap recognition state with the 1-nt gapped DNA (**Figure 4C-D**).

We then reassessed the loading efficiency of β-clamp basic patch mutant using a DNA substrate containing a large gap. In contrast to the severe defects observed on 6-nt gapped DNA, the loading efficiencies of the basic patch mutants increased modestly to ~50% of wild-type levels on this substrate. These results further underscore the importance of the β-clamp basic patch in clamp loading, particularly during the early stages of DNA recruitment (**Figure 4E**).

8. The intermediates depict a complete clamp-loading cycle

The eight cryo-EM 3D maps obtained with the 10-nt gapped DNA collectively describe a near-complete β-clamp loading cycle. Among these structures, six ternary clamp loader–clamp–DNA intermediates illustrate the progressive transition of the β-clamp gate from a fully open to a fully closed state as it

286 becomes loaded onto DNA (**Figure 5, Supplemental Video 3**). These intermediates are consistent with,
287 and complementary to, recently reported structures of the *E. coli* DnaX-complex loading β-clamp onto
288 tailed DNA substrtes[16,17]. Overall, the observed sequence of events resembles the multistep clamp
289 loading processes described for eukaryotic PCNA and the 9-1-1 clamp by RFC and Rad24-RFC,
290 respectively[13-15,31].
291
292 Across the six loading intermediates, the clamp loader components adopt highly similar conformations,
293 with $RMSD_{C\alpha}$ values ranging from 0.5 to 0.7 Å (**Figure 5A**–**B**). In the first conformer, the β-clamp gate is
294 open by ~22 Å—sufficient to accommodate passage of the ~20 Å-wide duplex DNA—and the 3′-dsDNA
295 has entered the clamp but remains tilted by ~22° relative to the clamp axis. We refer to this intermediate
296 as the "fully open, DNA unsettled" state (**Figure 5A**). In the second conformer, the DNA tilt decreases to
297 ~17°, yielding the "fully open, DNA settled" state. In the third conformer, the clamp gate narrows further
298 to ~8.5 Å, and the DNA tilt decreases slightly to ~16°.
299
300 In the fourth through sixth conformers, the clamp gate is fully closed, and the clamp progressively
301 dissociates from the DnaX-complex. From the fourth to the fifth conformer, the clamp tilts away from the
302 loader by ~4°, followed by an additional ~3° tilt from the fifth to the sixth conformer (**Figure 5B**).
303 Quantitative analysis of protein-protein interfaces reveals that, from the DNA gap recognition state to the
304 partially-closed clamp gate conformer, the interface area between DnaX3 and β2 increases modestly
305 from ~958 $Å^2$ to ~1097 $Å^2$, before decreasing to ~767 $Å^2$, ~613 $Å^2$, and finally to zero in the subsequent
306 fully closed conformers. In contrast, the interface between the δ′ subunit and β2 remains relatively
307 constant (~950 $Å^2$) across the first four conformers, then decreases sharply to ~340 $Å^2$ in the first fully
308 closed conformer and is completely lost in the final two conformers (**Figure 5B**).
309
310 In addition to the seven clamp loading intermediates, we captured a DnaX-complex-only structure at 2.95
311 Å resolution. This structure was initially presumed to represent a pre-loading state; however, careful
312 nucleotide modeling revealed that, whereas all ATP-binding sites in the 12 clamp–clamp loader–DNA
313 complexes (with either 1-nt or 10-nt gapped DNA) contain ATPγS, the DnaX-complex-only structure
314 contains ADP at the ATPase sites of DnaX subunits 1 and 3, with ATPγS bound at subunit 2 (**Figure**
315 **S6**). These observations indicate that ATPγS hydrolysis occurred following clamp loading and clamp
316 loader ejection.
317
318 This finding is notable given that ATPγS is considered a slowly hydrolyzable ATP analog[12-15]. The
319 observed hydrolysis suggests that the *E. coli* DnaX-complex is a more robust ATPase than its eukaryotic
320 counterpart, consistent with our biochemical results, showing that, although DnaX-complex does not

321 unwind DNA at nicks or very small gaps, it can nevertheless load the β-clamp onto such substrates given
322 sufficient time (**Figure 3A**).
323
324 **9. The DNA recessed 5′ end does not stimulate clamp loading activity of DnaX-complex**
325 In the absence of DNA, clamp loaders from *E. coli*, yeast and humans adopt broadly similar overall
326 architectures (**Figure S7A**). Upon DNA binding, however, the eukaryotic RFC clamp loader undergoes
327 conformational changes that expose basic residues on the Rfc1 AAA+ module, together with the unique
328 Rfc1 BRCT domain, forming a large, highly positively charged surface at the shoulder. This surface
329 serves as a secondary binding site that stably engages the 5′-dsDNA segment during clamp
330 loading[12,17,31,35]. In contrast, with either 1-nt or 10-nt gapped DNA, the 5′-dsDNA remains largely
331 disordered at the shoulder region of the bacterial DnaX-complex, as described above.
332
333 Electrostatic surface potential analysis further reveals that the shoulder region of the DnaX-complex is
334 largely neutral or weakly negatively charged, in stark contrast to the highly positively charged shoulder of
335 eukaryotic RFC (**Figures 6A and S7B-D**). This difference suggests that the bacterial clamp loader lacks
336 a dedicated shoulder DNA-binding site capable of stably engaging the 5′-dsDNA.
337
338 If the DnaX-complex does not possess a functional shoulder DNA-binding site, then the presence of a 5′-
339 recessed end should not enhance clamp loader-DNA interactions or clamp loading efficiency. To test this
340 prediction, we measured the affinity of the γ-complex for three different DNA substrates using a
341 fluorescence polarization-based binding assay with Cy3-labeled DNA (see **STAR METHODS**): (1) a
342 primer/template (p/T) DNA containing only a recessed 3′ end, (2) a 10-nt gapped DNA containig both
343 recessed 3′ and 5′ ends, and (3) a 30-nt gapped DNA containing both recessed ends (**Figure 6B**). The
344 apparent dissociation constant ($^{App}K_d$) for these substrates were 117.8 ± 11.1 nM, 97.2 ± 13.7 nM, and
345 93.7 ± 6.7 nM, respectively, indicating that the presence of a recessed 5′ end does not significantly
346 enhance DNA binding by the DnaX-complex.
347
348 We examined whether the presence of a 5′-recessed end influences clamp loading activity using a clamp
349 loading-dependent primer extension assay. In this assay, DNA synthesis by Pol III requires loading of the
350 β-clamp and thus serves as a proxy for clamp loading efficiency (see **STAR Methods**). We used two
351 DNA substrates. The first was a p/T DNA, consisting of a recessed 5′ end ^{32}P-labeled 30-nt primer (Pri-1)
352 annealed to a 100-nt template biotin-labeled at both ends, thereby containing only a 3′-recessed end.
353 The second was a 45-nt gapped DNA, generated by annealing an additional 25-nt primer (Pri-2),
354 thereby creating both 3′- and 5′-recessed ends. Streptavidin (SA) was added to block the DNA ends and
355 prevent the β-clamp from diffusing off the DNA (**Figures 6C and S8A**). Sufficient Pol III was added to
356 ensure that the reaction was rate-limited only by clamp loading. The p/T and gapped DNAs were not

extended by Pol III in the absence of clamp loading under our conditions and thus serve as negative controls. Both substrates were extended in the presence of clamp loading. We found that the amount of synthesized DNA was similar for both substrates, with the p/T DNA yielding a slightly higher amount (**Figure 6C**). This result is again consistent with the structural observations.

We further examined stimulation of DnaX-complex ATPase by DNA substrates containing a nick or gaps of different sizes in the presence of β-clamp (**Figure S8B**). Small and larger gapped DNAs produced similar levels of ATPase hydrolysis, whereas a 5-nt gapped DNA yielded a measurably lower ATPase activity. Considering that clamp loading efficiency onto nicked or 2-nt gapped DNA is markedly lower than onto DNA with 4-nt or larger gap (**Figure 3A**), these results imply that a significant fraction of ATP hydrolysis might be attributed to failed DNA bending events during clamp loading, even though these substrates consume a similar amount of ATP as the 10-nt gapped DNA. By contrast, the reduced ATP consumption observed with the 5-nt gapped DNA may indicate that its 5′-dsDNA segment can more readily bend back to engage the β-clamp basic patch (as observed in the state 2 structures captured with 1-nt gapped DNA), thereby facilitating clamp loading, specifically the entry of the 3′-dsDNA into clamp–clamp loader chamber.

DISCUSSION

In this work, we uncover a fundamental mechanistic difference between the bacterial and eukaryotic clamp loading onto nicked and small-gapped DNA substrates. A minimum stretch of ~ 6 nt of ssDNA is generally required to thread through the clamp loader chamber to enable recognition and binding of a recessed DNA 3′ end for clamp loading. When the gap is smaller than this threshold, eukaryotic RFC widens the gap by unwinding the DNA from the 3′ end, whereas the bacterial DnaX-complex instead sharply bends the 5′-dsDNA by ~150º, forcing the 3′-dsDNA into the clamp chamber without detectable strand separation. Despite the absence of DNA unwinding activity, the δ-subunit residue Y316 of the DnaX-complex approaches and interacts with the recessed 3′ end, consistent with a role in DNA end recognition rather than strand separation.

Importantly, these mechanistic distinctions are based on the substrates and conditions examined in this study. While our data show no evidence of DNA unwinding by the bacterial clamp loader under these conditions, we cannot exclude the possibility that DNA bending also occurs in eukaryotic systems or that DNA unwinding may contribute to bacterial clamp loading under alternative physiological conditions, in the presence of additional factors, or with different DNA substrates.

Small ssDNA gaps and nicks are common intermediates generated during DNA damage processing and repair. The ability of the DnaX-complex to load the β-clamp efficiently at such sites—without requiring

393 DNA unwinding or a dedicated shoulder DNA-binding site—suggests a mechanism that may be
394 particularly well suited for coordinating DNA repair synthesis, and would be consistent with repair
395 deficiency in yeast when using RFC that cannot bind a small gap due to loss of its 5′-dsDNA binding
396 domain (N-terminal truncation)[14,38]. Consistent with this idea, the *E. coli* β-clamp is known to play central
397 roles in recruiting and coordinating multiple DNA repair and translesion synthesis polymerases, as well
398 as other repair-associated factors[39-49]. Sharp DNA bending at small gaps may therefore facilitate rapid
399 clamp loading and polymerase exchange at sites of damage, enabling efficient downstream repair.
400
401 **Proposed β-clamp loading mechanism by DnaX-complex**
402 The bacterial clamp loader appears to load the β-clamp in a DNA structure–dependent manner. During
403 normal bacterial replication, Okazaki fragments are typically 1–2 kb long, such that the preceding
404 Okazaki fragment (i.e., 5′-dsDNA) is too distant to influence clamp loading and can effectively be
405 ignored. Under these conditions, the 3′-dsDNA first binds in a tilted orientation to the basic patch on the
406 outer surface of the open β-clamp (**Figure 7**). The DnaX-complex then engages the recessed primer 3′
407 end via the δ-subunit Y316, allowing the 3′-dsDNA to diffuse toward the higher-affinity binding site within
408 the β-clamp chamber through a series of steps captured here and in recent studies[16,17].
409
410 When the DnaX-complex encounters a nick or a small gap (<6 nt), the loading pathway diverges. In
411 contrast to eukaryotic RFC, which can unwind the DNA 3′ end by up to 6 bp using the Rfc1 separation
412 pin W638—a two-ring aromatic residue—while the corresponding residue in *E. coli*, δ-subunit Y316, is a
413 single-ring aromatic residue and does not unwind DNA[14]. Instead, the bacterial clamp loader appears to
414 have evolved a distinct strategy that may be particularly suited for recruiting repair polymerases (Pol I, II,
415 IV, and V) to sites of DNA damage[47,50-53].
416
417 At small gaps, the primer 3′ end is initially sterically hindered from entering the DnaX-complex chamber
418 because the adjacent 5′-dsDNA segment is too bulky to be accommodated. In the absence of stable 5′-
419 dsDNA binding at the clamp loader shoulder, the 5′-dsDNA bends sharply down toward the 3′-dsDNA,
420 generating a U-shaped DNA conformation (**Figure 7**). This sharp bending has two important
421 consequences. First, it exposes the recessed primer 3′ end, facilitating its recognition by δ Y316 and its
422 subsequent entry and proper positioning within the clamp loader chamber (**Figure S4**). Second, the
423 bending-induced strain within the DNA promotes the displacement of the 3′-dsDNA from the external β-
424 clamp binding site and drives its insertion into the β-clamp chamber.
425
426 Following entry of the 3′-dsDNA into the clamp, the 5′-dsDNA binds transiently to the β-clamp basic patch
427 vacated by the 3′-dsDNA, further promoting clamp closure. Electrostatic attraction between the
428 negatively charged DNA backbone and the positively charged interior surface of the β-clamp is expected

429 to drive full or near-complete gate closure, analogous to mechanisms proposed for PCNA and the 9-1-1
430 clamp[12-15,18,25-27,31]. Clamp closure is then coupled to ATP hydrolysis, triggering dissociation of the DnaX-
431 complex. Upon clamp loader release, the bent DNA is expected to relax back to a linear configuration,
432 allowing the β-clamp to fully encircle the DNA. Such a mechanism is likely advantageous at
433 discontinuous DNA substrates encountered during DNA repair, where rapid clamp loading and
434 polymerase exchange are required. Consistent with this model, our loading assays demonstrate that the
435 β-clamp can be successfully loaded onto a 1-nt gapped DNA substrate (**Figure 3A**).
436
437 **The β-clamp external DNA binding site may compensate for the lack of a shoulder 5′ DNA site in**
438 **DnaX-complex**
439 Sharp DNA bending generally requires at least two spatially separate DNA-binding sites. For example,
440 during replication origin recognition, yeast origin DNA is bent by ~50º by the origin recognition complex
441 (ORC), which engages DNA at two distinct sites—one within the ORC ring and the other on the external
442 surface formed by Orc5 and Orc6[54,55]. Similarly, eukaryotic RFC employs two dsDNA-binding sites to
443 load PCNA onto gapped DNA: the primary site within the chamber that binds the 3′-dsDNA, and a
444 secondary, highly positively charged shoulder site that engages the 5′-dsDNA[13,15,25-27].
445
446 In contrast, the *E. coli* DnaX-complex lacks a comparable positively charged shoulder region, and the 5′-
447 dsDNA does not stably bind there. Instead, our structures and biochemical data indicate that the β-clamp
448 itself has evolved a conserved basic patch on its external surface that can bind DNA, providing the
449 second DNA-binding site for the bacterial clamp loading system (**Figures 2D-E** and **S7A-C**). This β-
450 clamp basic patch may therefore functionally compensate for the absence of a shoulder 5′-dsDNA-
451 binding site in the DnaX-complex.
452
453 Notably, the RFC shoulder site includes the Rfc1 N-terminal BRCT domain, which is unique to
454 eukaryotes and has been proposed to function in initial DNA recruitment[3,15,25-27]. By analogy, the β-clamp
455 basic patch may serve a related role in bacterial clamp loading by stabilizing transient DNA interactions
456 during recruitment and loading. Thus, although the molecular components differ, both systems appear to
457 utilize two DNA-binding sites to achieve clamp loading at nicks and gaps, highlighting a convergent
458 functional strategy implemented through distinct structural solutions.
459
460 **DnaX-complex is anchored to the replication fork for repeated clamp loading**
461 The DnaX-complex functions as more than a clamp loader; it also serves as a central organizer of the
462 bacterial replisome, coordinating helicase and polymerase activities at the replication fork[56-59] (**Figure**
463 **S9**). This multifunctionality is conferred by the CTDs of the three τ subunits (τ_{CTDs}), which mediate
464 interactions with multiple replication proteins[60]. One τ_{CTD} anchors the leading strand Pol III, a second τ_{CTD}

465 anchors the lagging-strand Pol III, and the third can recruit an additional polymerase, providing backup or
466 facilitating completion of lagging strand synthesis when polymerase exchange is required[61,62].
467
468 In addition to polymerase tethering, the DnaX-complex is linked to the replication fork through its χ
469 subunit, which binds the SSB[36,57]. This interaction helps position the clamp loader at sites of active DNA
470 synthesis and likely promotes efficient and repeated β-clamp loading at newly generated primer-template
471 junctions. In this study, we visualized for the first time the χψ heterodimer assembled within the DnaX-
472 holo-complex during β-clamp loading (**Figure S9**), providing structural context for earlier biochemical and
473 solution studies[36,57,63].
474
475 The ability of the DnaX-complex to remain anchored at the replication fork offers a mechanistic
476 explanation for how clamp loading can be efficiently coupled to ongoing DNA synthesis. By maintaining
477 proximity to a primer-template junction and to SSB-coated ssDNA, the DnaX-complex is well positioned
478 to rapidly respond to newly formed primers during replication and repair, ensuring timely loading of the β-
479 clamp as needed.
480
481 Beyond its biological implications, the distinct clamp-loading mechanism described here may also have
482 biomedical relevance. The reliance of bacterial clamp loading on a conserved β-clamp DNA-binding
483 patch and on sharp DNA bending represents features that are absent from eukaryotic clamp loaders.
484 These mechanistic differences raise the possibility that bacterial clamp loading could be selectively
485 targeted, providing a potential avenue for the development of species-specific antibacterial strategies
486 that interfere with DNA replication and repair without affecting eukaryotic counterparts.
487
488 **Limitations of the Study**
489 This study reveals a distinct mechanism by which the *E. coli* DnaX-complex loads the β-clamp onto
490 nicked and small-gapped DNA substrates (<6 nt), characterized by sharp DNA bending rather than DNA
491 unwinding, as observed for eukaryotic RFC. Although these features are well supported by in vitro cryo-
492 EM and biochemical analyses, the biological consequences of these mechanistic differences in vivo
493 remain to be fully established. Moreover, we cannot exclude the possibility that DNA bending also occurs
494 in eukaryotic systems, or that DNA unwinding may contribute to bacterial clamp loading under
495 physiological conditions or with DNA substrates not examined here.
496
497 In particular, the physiological roles of the conserved basic patch on the β-clamp and of the δ-subunit
498 residue Y316 during DNA replication and repair warrant further investigation. While our structural and
499 biochemical data indicate that these elements are important for DNA recognition and clamp loading at
500 small gaps, their precise contributions to cellular DNA repair pathways remain unknown. Determining

501 how these features influence polymerase selection, clamp dynamics, and repair efficiency in vivo will be
502 an important direction for future studies.
503
504 In addition, although our experiments capture multiple clamp-loading intermediates under defined in vitro
505 conditions, it remains possible that alternative DNA substrates, accessory factors, or cellular
506 environments could modulate the clamp loading pathway. Thus, while our results establish a mechanistic
507 framework for understanding bacterial clamp loading at nicks and small gaps, further work will be
508 required to define how this mechanism operates within the full cellular replication and repair machinery.
509

510 **STAR★METHODS**

511 Detailed methods are provided in the online version of this paper and include the following:

512 - KEY RESOURCES TABLE
513 - RESOURCE AVAILABILITY
514 - Lead contact
515 - Materials availability
516 - Data and code availability
517 - EXPERIMENTAL MODEL AND SUBJECT DETAILS
518 - METHOD DETAILS
519 - Protein expression and purification
520 - β-clamp mutants preparation
521 - γ-complex mutant preparation
522 - Gel filtration-based analysis of β-clamp loading
523 - Fluorescence polarization-based DNA binding assay
524 - Rate of clamp loading onto primed versus gapped DNA
525 - Cryo-EM grids preparation and data collection
526 - Image processing and 3D reconstruction
527 - Model building, refinement, and validation
528 - QUANTIFICATION AND STATISTICAL ANALYSIS
529

530 **SUPPLEMENTAL INFORMATION**

531 Supplemental Information can be found online at:
532

533 **ACKNOWLEDGMENTS**

534 Cryo-EM micrographs were collected at the David Van Andel Advanced Cryo-Electron Microscopy Suite
535 in the Van Andel Institute. We thank G. Zhao and X. Meng for assistance with data collection. This work

was supported by U.S. National Institutes of Health grants GM115809 (to M.E.O.) and GM131754 (to H.L.), the Howard Hughes Medical Institute (to M.E.O.), and the Van Andel Institute (to H.L.).

AUTHOR CONTRIBUTIONS

F.Z., M.E.O., and H.L. designed research; F.Z., N.Y., R.E.G. and M.L. performed research; F.Z., R.E.G., N.Y.Y., M.L., M.E.O., and H.L. analyzed the data; F.Z., M.E.O., and H.L. wrote the manuscript with input from all authors.

DECLARATION OF INTERESTS

The authors declare no competing interests.

547 **STAR★METHODS**

548 **KEY RESOURCES TABLE**

REAGENT or RESOURCE	SOURCE	IDENTIFIER
Antibodies		
Bacterial and virus strains		
E. coli DH5α competent cells	Thermo Fisher Scientific	Cat# 18265017
E. coli BL21(DE3) competent cells	Thermo Fisher Scientific	Cat# EC0114
Chemicals, peptides, and recombinant proteins		
dNTPs	Cytiva	Cat# 28406551
[γ-^{32}P] ATP	PerkinElmer Life Sciences	Cat# BLU002Z500UC
ATPγS	Millipore Sigma	Cat# 11162306001
Anti-FLAG beads	Millipore Sigma	Cat# A36797
Bradford protein assay kit	Bio-Rad	Cat# 5000001
Deposited data		
Cryo-EM map of DnaX-complex–β-clamp–1-nt gapped DNA at state 1 conformer 1	This study	EMDB: EMD-71013
Cryo-EM map of DnaX-complex–β-clamp–1-nt gapped DNA at state 1 conformer 2	This study	EMDB: EMD-71014
Cryo-EM map of DnaX-complex–β-clamp–1-nt gapped DNA at state 1 conformer 3	This study	EMDB: EMD-71015
Cryo-EM map of DnaX-complex–β-clamp–1-nt gapped DNA at state 2 conformer 1	This study	EMDB: EMD-71016
Cryo-EM map of DnaX-complex–β-clamp–1-nt gapped DNA at state 2 conformer 2	This study	EMDB: EMD-71017
Cryo-EM map of DnaX-complex alone	This study	EMDB: EMD-71018
Cryo-EM map of DnaX-complex–β-clamp–10-nt gapped DNA at state 1 DNA recognition	This study	EMDB: EMD-71021
Cryo-EM map of DnaX-complex–β-clamp–10-nt gapped DNA at state 2 conformer 1 fully open_DNA unsettled	This study	EMDB: EMD-71022
Cryo-EM map of DnaX-complex–β-clamp–10-nt gapped DNA at state 2 conformer 2 fully open_DNA settled	This study	EMDB: EMD-71023

Cryo-EM map of DnaX-complex–β-clamp–10-nt gapped DNA at state 2 conformer 3 partially closed	This study	EMDB: EMD-71024
Cryo-EM map of DnaX-complex–β-clamp–10-nt gapped DNA at state 2 conformer 4 fully closed_1	This study	EMDB: EMD-71025
Cryo-EM map of DnaX-complex–β-clamp–10-nt gapped DNA at state 2 conformer 5 fully closed_2	This study	EMDB: EMD-71026
Cryo-EM map of DnaX-complex–β-clamp–10-nt gapped DNA at state 2 conformer 6 fully closed_3	This study	EMDB: EMD-71027
Atomic model of DnaX-complex–β-clamp–1-nt gapped DNA at state 1 conformer 1	This study	PDB: 9OYB
Atomic model of DnaX-complex–β-clamp–1-nt gapped DNA at state 1 conformer 2	This study	PDB: 9OYC
Atomic model of DnaX-complex–β-clamp–1-nt gapped DNA at state 1 conformer 3	This study	PDB: 9OYD
Atomic model of DnaX-complex–β-clamp–1-nt gapped DNA at state 2 conformer 1	This study	PDB: 9OYE
Atomic model of DnaX-complex–β-clamp–1-nt gapped DNA at state 2 conformer 2	This study	PDB: 9OYF
Atomic model of DnaX-complex alone	This study	PDB: 9OYG
Atomic model of DnaX-complex–β-clamp–10-nt gapped DNA at state 1 DNA recognition	This study	PDB: 9OYH
Atomic model of DnaX-complex–β-clamp–10-nt gapped DNA at state 2 conformer 1 fully open_DNA unsettled	This study	PDB: 9OYI
Atomic model of DnaX-complex–β-clamp–10-nt gapped DNA at state 2 conformer 2 fully open_DNA settled	This study	PDB: 9OYJ
Atomic model of DnaX-complex–β-clamp–10-nt gapped DNA at state 2 conformer 3 partially closed	This study	PDB: 9OYK

Atomic model of DnaX-complex–β-clamp–10-nt gapped DNA at state 2 conformer 4 fully closed_1	This study	PDB: 9OYL
Atomic model of DnaX-complex–β-clamp–10-nt gapped DNA at state 2 conformer 5 fully closed_2	This study	PDB: 9OYM
Atomic model of DnaX-complex–β-clamp–10-nt gapped DNA at state 2 conformer 6 fully closed_3	This study	PDB: 9OYN
Oligonucleotides		
gBlocks HiFi gene fragments	Integrated DNA Technologies	N/A
5′- GGCTCGCTACGGCTATACGG/Cy3/ -3′ (Primer 1 for 1-nt and 10-nt gapped DNA in cryo-EM, also for binding affinity assay)	Integrated DNA Technologies	N/A
5′- GATTCGTATCGCCTATACCG -3′ (Primer 2 for 1-nt and 10-nt gapped DNA in cryo-EM, also for binding affinity assay)	Integrated DNA Technologies	N/A
5′- CGGTATAGGCGATACGAATCTCCGTA TAGCCGTAGCGAGCC -3′ (Tmpl_41-nt for 1-nt gapped DNA in cryo-EM)	Integrated DNA Technologies	N/A
5′- CGGTATAGGCGATACGAATC$(T)_{10}$CCGTA TAGCCGTAGCGAGCC -3′ (Tmpl_50-nt for 10-nt gapped DNA in cryo-EM, also for binding affinity assay)	Integrated DNA Technologies	N/A
5′- CGGTATAGGCGATACGAATC$(T)_{30}$CCGTA TAGCCGTAGCGAGCC -3′ (Tmpl_70-nt for binding affinity assay)	Integrated DNA Technologies	N/A
5′- BioTEG/GGGAAGGGCGATCGGTGCGGG CCTCTTCGCTATTACGCCAGCTGGCGAAA GGGGGATGTGCTGCAAGGCGATTAAGTTG GGTAACGC -3′ (M13 primer for loading assay)	Integrated DNA Technologies	N/A

5′- BioTEG/CTGGATGAGTTGAGTGGACGGC TGCAGCAAGTCACCAATGTCTAAGAGTTC GTATTATGCCTACACTGGAGTACCGGAGCA TCGTCGTGACTGGGAAACT/BioTEG/ -3′ (replication template)	Integrated DNA Technologies	N/A
5′- AGTTTCCCAGTCACGACGATGCTCCGG TAC -3′ (replication primer 1)	Integrated DNA Technologies	N/A
5′- GCAGCCGTCCACTCAACTCATCCAG -3′ (replication primer 2)	Integrated DNA Technologies	N/A
Recombinant DNA		
cAMP-dependent protein kinase	Kelman et al.,[64] 1995	Sigma # P2645
DnaX-complex expression plasmids	Onrust et al.,[29] 1995	Addgene numbers for expression of the five subunits: (E coli DnaX tau only, 237237; Ec holA pET11a, 237233; Ec holB pET11a, 237234; Ec holC pET 3c, 237235; Ec hold pET 3c, 237236)
Pol III αε expression plasmids	Studwell et al.,[65] 1990	Addgene
SSB expression plasmid	Studwell et al.,[65] 1990	Addgene # 237240
β-clamp expression plasmid	Studwell et al.,[65] 1990	Addgene # 237238
Kinase tagged β-clamp expression plasmid	Kelman et al 1995,[66]	Addgene # 237239
pUC19 plasmid with nick (for loading assay): GCTCTTC***GC***TGAGG CGAGAAGCGACTCC	This study	By restriction enzyme Nt. BspQ1
pUC19 plasmid with 1-nt gap (for loading assay): GCTCTTCG***c***TGAGG CGAGAAGCGACTCC	This study	By restriction enzymes Nt. BspQ1 and Nb. BbvC1
pUC19 plasmid with 2-nt gap (for loading assay): GCTCTTC***gc***TGAGG CGAGAAGCGACTCC	This study	By restriction enzyme Nt. BspQ1 and Nb. BbvC1

pUC19 plasmid with 4-nt gap (for loading assay): GCTCTTCC***gctg***CATTC CGAGAAGGCGACGTAAG	This study	By restriction enzyme Nt. BspQ1 and Nb. Bsm I
pUC19 plasmid with 6-nt gap (for loading assay): GCTCTTCC***gctaag***CATTC CGAGAAGGCGATTCGTAAG	This study	By restriction enzyme Nt. BspQ1 and Nb. Bsm I
pUC19 plasmid with 8-nt gap (for loading assay): GCTCTTCC***gctaaaag***CATTC CGAGAAGGCGATTTTCGTAAG	This study	By restriction enzyme Nt. BspQ1 and Nb. Bsm I
Software and algorithms		
SerialEM	Mastronarde,[67] 2003	https://bio3d.colorado.edu/SerialEM/
cryoSPARC v4.3.1 and v4.5.3	Punjani et al.,[68] 2017	https://cryosparc.com/
Relion 5.0	Scheres,[69] 2012	https://relion.readthedocs.io/en/release-5.0/
MotionCor2	Zheng et al.,[70] 2017	https://emcore.ucsf.edu/ucsf-software
CTFFIND4	Rohou and Grigorieff,[71] 2015	https://grigoriefflab.janelia.org/ctffind4
Topaz	Bepler et al.,[72] 2019	https://cb.csail.mit.edu/cb/topaz/
PyEM	Asarnow et al.,[73] 2019	https://zenodo.org/record/3576630#.ZDbbk-zMLsc
UCSF Chimera	Pettersen et al.,[74] 2004	http://www.cgl.ucsf.edu/chimera/
UCSF Chimera X	Goddard et al.,[75] 2018	https://www.cgl.ucsf.edu/chimerax/
Coot	Emsley et al.,[76] 2010	http://www2.mrc-lmb.cam.ac.uk/personal/pemsley/coot
PHENIX	Adams et al.,[77] 2010	https://phenix-online.org
Other		
Quantifoil Au R1.2/1.3 300 mesh grids	SPI Supplies	Cat# 4230G-XA

Quantifoil UltrAu R1.2/1.3 300 mesh grids	SPI Supplies	Cat# 4976G-FA
Gatan Solarus plasma cleaner 950	Gatan	N/A
Vitrobot Mark IV	Thermo Fisher Scientific	N/A
Talos Arctica Cryo-TEM	Thermo Fisher Scientific	N/A
Titan Krios G2 Cryo-TEM	Thermo Fisher Scientific	N/A

RESOURCE AVAILABILITY

Lead contact. Further information and requests for reagents and resources should be directed to, and will be fulfilled by, the Lead Contact, Huilin Li (Huilin.Li@vai.org).

Materials availability. All plasmid clones used to express the proteins in this study are available upon request without restrictions, although a material transfer agreement (MTA) may be required.

Data and code availability

- Five conformers of the DnaX-complex bound to β-clamp and 1-nt gapped DNA (states 1 and 2) have been deposited in the Electron Microscopy Data Bank under accession codes EMD-71013, EMD-71014, EMD-71015, EMD-71016, and EMD-71017. The corresponding atomic models have been deposited in the Protein Data Bank under accession codes 9OYB, 9OYC, 9OYD, 9OYE, and 9OYF. These data will be publicly available upon publication.
- One DnaX-complex–alone structure and seven conformers of DnaX-complex bound to β-clamp and 10-nt gapped DNA have been deposited in the Electron Microscopy Data Bank under accession codes EMD-71018, EMD-71021, EMD-71022, EMD-71023, EMD-71024, EMD-71025, EMD-71026 and EMD-71027. The corresponding atomic models have been deposited in the Protein Data Bank under accession codes 9OYG, 9OYH, 9OYI, 9OYJ, 9OYK, 9OYL, 9OYM, and 9OYN. These data will be publicly available upon publication.
- This paper does not report original code.
- Clones used for expression of factors in this study have been deposited in the Addgene repository.
- Any additional information required to reanalyze the data reported in this work will be available from the Lead Contact upon request.

EXPERIMENTAL MODEL AND STUDY PARTICIPANT DETAILS

Bacterial strains

577 Expression plasmids encoding the *E. coli* DnaX-complexes—specifically the γ-complex ($\delta\gamma_3\delta'\chi\psi$), used
578 for biochemical studies, and the τ-complex ($\delta\tau_3\delta'\chi\psi$), used for cryo-EM studies—as well as the β-clamp
579 and its related mutants, SSB, and Pol III αε complex, were generated as described previously[29,65]. All
580 proteins were expressed from the plasmids listed in the **KEY RESOURCES TABLE** following
581 transformation into *E. coli* BL21(DE3) cells (Thermo Fisher Scientific) and cultured in LB media.
582
583 **METHOD DETAILS**
584 **Protein expression and purification**
585 The *E. coli* DnaX-complex subunits δ, γ, τ, δ′, ψ, and χ were purified as described previously[29]. The β-
586 clamp, Pol III αε complex, and SSB were purified as described previously[65]. The clamp loader γ-complex
587 was reconstituted from purified subunits and further purified by ion-exchange chromatography using a
588 Cytiva MonoQ column as described[29]. Briefly, purified subunits (1–4 mg each in approximately 3 mL of
589 20 mM Tris-HCl, pH 7.5, 1 mM DTT, 0.5 mM EDTA, 10% glycerol) were mixed at a molar ratio of
590 $\delta:\gamma_3:\delta':\psi:\chi$ = 1.5:1:1.5:1.5:2. The subunit mixture was incubated for 30 min at 15 °C and then applied to a
591 1-mL MonoQ column (GE Healthcare, Chicago, IL). Proteins were eluted using a 10-column-volume
592 linear gradient of Buffer A (20 mM Tris-HCl, pH 7.5, 0.5 mM DTT, 1 mM EDTA, 10% glycerol)
593 supplemented with 50 mM NaCl, and 0.2-mL fractions were collected. Fractions were analyzed by 12%
594 SDS–PAGE. The γ-complex eluted at approximately 0.4 M NaCl, whereas individual subunits and
595 subcomplexes eluted earlier. The τ-complex was reconstituted and purified in the same procedure,
596 except that τ was substituted for γ. Peak fractions of each complex were pooled and dialyzed against
597 Buffer A supplemented with 50 mM NaCl, aliquoted, snap-frozen in liquid nitrogen, and stored at −80 °C.
598
599 **Mutant β-clamp preparation**
600 gBlocks HiFi gene fragments were designed to contain the full-length *dnaN* gene, including an N-terminal
601 3×FLAG tag followed by a protein kinase A recognition site (LRRASLG)[66]. The gBlocks were cloned into
602 pRSFDuet (Novagen, Burlington, MA) that had been digested with NcoI-HF and BamHI-HF and treated
603 with alkaline phosphatase. This strategy was used to generate wild-type β-clamp ($\beta\text{-clamp}_{WT}$) as well as
604 two mutants containing three amino acid substitutions: R96A, R103A, and R105A ($\beta\text{-clamp}_{Mut1}$) and
605 R96E, R103E, and R105E ($\beta\text{-clamp}_{Mut2}$).
606
607 The gBlocks were dissolved in 20 mM Tris-acetate (pH 7.9), 50 mM K-acetate, 10 mM $MgCl_2$, and 100
608 μg/mL BSA, followed by digestion with NcoI-HF and BamHI-HF. The resulting plasmids were
609 transformed into *E. coli* DH5α cells (ThermoFisher Scientific, Waltham, MA), plated on LB agar
610 containing kanamycin (50 μg/mL), and incubated overnight at 37 °C. Colonies were screened by
611 miniprep and NcoI-HF/BamHI-HF restriction digestion on native agarose gels, followed by maxiprep and
612 verification of the entire *dnaN* coding sequence by Sanger sequencing (Genewiz, South Plainfield, NJ).

613
614 Sequence-verified plasmids were transformed into *E. coli* BL21(DE3) cells, and 3 L cultures were grown
615 to an OD_{600} of 0.6 before induction with 2 mM IPTG for 12 h at 15 °C. Cells were harvested by
616 centrifugation, resuspended in Buffer A supplemented with 750 mM NaCl, and lysed using an Avestin
617 EmulsiFlex-C-50 (Ottawa, ON, Canada). PMSF was added to a final concentration of 1 mM, and the
618 lysate was clarified by centrifugation at 12,500 rpm in an F14-6×250 rotor (ThermoFisher Scientific,
619 Waltham, MA) at 4 ºC for 1 h.
620
621 Anti-FLAG affinity purification was performed by incubating the clarified supernatant (~400 mL) with 5 mL
622 anti-FLAG resin for 30 min at 4 °C with gentle mixing. The beads were collected by centrifugation and
623 washed once with 450 mL Buffer A containing 300 mM NaCl, followed by three additional wash with 400
624 mL Buffer A containing 300 mM NaCl. The final bead pellet was resuspended in 15 mL Buffer A
625 containing 50 mM NaCl and loaded onto an XK-16/20 column (Cytiva, Marlborough, MA). The column
626 was washed with 15 mL Buffer A containing 1 M NaCl and then equilibrated with Buffer A containing 50
627 mM NaCl. Bound proteins were eluted in four successive 30-min pulses of 5 mL Buffer A containing 50
628 mM NaCl and 0.23 mg/mL 3×FLAG peptide. Eluted fractions were analyzed by SDS–PAGE, pooled,
629 dialyzed against Buffer A, concentrated to approximately 2 mg/mL, and stored at −80 °C.
630
631 **Mass photometry**
632 Data were collected using a OneMP mass photometer (Refeyn), calibrated with bovine serum albumin
633 (66 kDa), β-amylase (224 kDa), and thyroglobulin (670 kDa). Movies were acquired for 6,000 frames (60
634 s) using AcquireMP software (version 2.4.0) with default settings. Final protein concentrations were
635 empirically adjusted to achieve approximately 75 binding events per second. Peak mass values are
636 expected to fall within ~5% error. Raw data were converted to frequency distributions using Prism 9
637 (GraphPad) and a bin size of 10 Da.
638
639 **Mutant γ subunit preparation**
640 The δ-subunit Y316A mutant was generated using a HiFi DNA fragment encompassing the region of
641 *holA* (gene encoding δ) from the internal AflII site to the BamHI site downstream of the stop codon,
642 including placement of a C-terminal 3×FLAG tag. This gBlock was inserted into AflII/BamHI-digested
643 pET11-holA to generate pET11-holA(Y316A). The full sequence of the mutant *holA* gene was verified by
644 Sanger sequencing.
645
646 The pET11-holA(Y316A) plasmid was transformed into *E. coli* Bl21(DE3) cells, and 12 L cultures were
647 grown under ampicillin selection, induced with 2 mM IPTG, and lysed in an Avestin EmulsiFlex-C-50

648 (Ottawa, ON, Canada). The δ Y316A protein was purified as described above for the β-clamp mutants,
649 concentrated, and stored at −80 °C.
650
651 The γ-complex containing the δ Y316A mutation was reconstituted by mixing purified δ Y316A mutant
652 with γ, δ‘, χ, and ψ subunits and purified as described previously[63] and as briefly outlined above.
653
654 **Construction of DNA substrates for the β-clamp loading assay**
655 pUC19 plasmid DNA was engineered to generate nicked or gapped DNA substrates of defined gap sizes
656 using one or two nicking endonucleases. The required insertions into pUC19 are listed in the **KEY**
657 **RESOURCES TABLE**. The nicking enzymes cut the same DNA strand, producing a short single-
658 stranded region that can be released from the circular plasmid to generate a nick or gap of defined
659 length.
660
661 For generation of 1- and 2-nt gapped DNA substrates, Nb.BbvCI and Nt.BspQI were used. For
662 generation of 4-, 6-, and 8-nt gapped DNA substrates, Nb.BsmI and Nt.BspQI were used. To generate
663 each gapped circular DNA, 43 µg of plasmid DNA was digested in a reaction containing 50 mM Tris-HCl
664 (pH 7.9), 100 mM NaCl, 10 mM $MgCl_2$, and 100 µg/mL BSA with 40 U each of the nicking enzymes. For
665 1- and 2-nt gapped DNA, Nb.BbvCI and Nt.BspQI digestions were performed sequentially at 37 ºC and
666 50 ºC, respectively. For 4-, 6- and 8-nt gapped DNA, Nt.BspQI and Nb.BsmI digestions were performed
667 sequentially at 50 ºC and 65 ºC, respectively.
668
669 Following digestion, enzymes were heat-inactivated at 80 ºC for 30 min, and reactions were terminated
670 by addition of EDTA to a final concentration of 5 mM. For 4-, 6- and 8-nt gapped DNA substrates, a
671 complementary oligo trap was added (4-nt gap: 5'-TTCTTAGCTT-3'; 6-nt gap: 5'-TTCTTAGCTT-3'; 8-nt
672 gap: 5'-TCTTTTAGCT-3'), and the reactions were heated to 55 ºC and then slowly cooled to room
673 temperature.
674
675 Approximately 25 µg of each reaction was purified using a spin column, and DNA was eluted in three
676 successive 20-µL elutions with 5mM Tris-HCl (pH 8.5) at 70 ºC. For the singly primed DNA substrate, a
677 biotinylated M13 primer was annealed to M13 ssDNA, followed by addition of a 5-fold molar excess of
678 streptavidin (**KEY RESOURCES TABLE**).
679
680 **Gel filtration–based β-clamp loading assay**
681 β-Clamp loading onto DNA was analyzed using the γ-complex, isotopically ^{32}P-labelled β-clamp, and the
682 corresponding clamp and clamp loader mutants. DNA-bound ^{32}P–β-clamp was separated from unbound
683 ^{32}P–β-clamp by gel filtration through a 5-mL Bio-Gel A15m column, essentially as described previously[30].

684 Briefly, β-clamp was radiolabeled by incubating 1 nmol FLAG–kinase–tagged wild-type or mutant β-
685 clamp in 100 μL buffer A containing 16.7 pmol γ-^{32}P-ATP and 0.45 μg protein kinase A (PKA; Sigma, St
686 Louis, MO) for 30 min at 37°C. Radiolabeled ^{32}P–β-clamp was separated from unincorporated ^{32}P-ATP
687 using a Cytiva G25 MicroSpin column equilibrated with buffer A supplemented with 50 mM NaCl. The
688 concentration and specific radioactivity of the purified ^{32}P–β-clamps were determined by Bradford assay
689 and liquid scintillation counting.
690
691 Clamp loading reactions contained 1 pmol (10 nM) pUC19 plasmid DNA with a nick or defined gap size,
692 or singly primed M13 ssDNA; 2 pmol (20 nM) ^{32}P–FLAG–PK–β-clamp (dimer); and varying
693 concentrations of γ-complex or their mutants, β-clamp$_{Mut1}$, β-clamp$_{Mut2}$ and γ-complex$_{Mut}$ in a total volume
694 of 100 μL Buffer B (20 mM Tris-HCl, pH7.5, 0.1 mM EDTA, 40 μg/mL BSA, 4% glycerol, 5 mM
695 dithiothreitol) supplemented with 8 mM $MgCl_2$, 2 mM ATP and 50 mM NaCl. Reactions were incubated
696 for 5 min at 37 °C. DNA-bound ^{32}P–β-clamp was separated from free ^{32}P–β-clamp by gel filtration
697 through a 5-mL Bio-Gel A15m column equilibrated with Buffer B supplemented with 8 mM $MgCl_2$ and 100
698 mM NaCl. Fractions (180 μL) were collected, and 150 μL aliquots were quantified by liquid scintillation
699 counting. Radioactivity was converted to femtomoles using the empirically determined specific
700 radioactivity of ^{32}P–β-clamp.
701
702 **Cryo-EM grids preparation and data collection**
703 The 1-nt and 10-nt gapped DNA substrates used for cryo-EM studies are shown in **Figures 1C** and **4A**.
704 *In vitro* assembly of clamp loading complexes containing purified *E. coli* DnaX-complex, β-clamp, and
705 DNA substrates followed our previously established reconstitution procedure for the yeast Polδ–PCNA–
706 DNA complex[78]. Briefly, either 13.0 μL of 1-nt gapped DNA at 7.1 μM or 8.0 μL of 10-nt gapped DNA at
707 11.5 μM were mixed with 1.0 μL β-clamp at 77.6 μM and incubated at 30 °C for 10 min. The DNA-clamp
708 mixtures, together with 1.0 μL of 10 mM ATPγS and 1.0 μL of 100 mM Mg-acetate, were then added to
709 7.1 μL DnaX-complex at a concentration of 8.4 μM. Ultrapure H_2O was added to bring the final reaction
710 volume to 20 μL. The mixture was incubated in an ice–water bath for an additional 10 min prior to cryo-
711 grid preparation.
712
713 Quantifoil Au or UltrAu R1.2/1.3 300-mesh grids were glow discharged for 0.5 min or 3 min, respectively,
714 using a Gatan Solarus plasma cleaner. Aliquots (3 μL) of the assembled clamp loading mixtures were
715 applied onto the grids, which were vitrification using a Vitrobot Mark IV (Thermo Fisher Scientific) under
716 the following conditions: blot time of 2 s for Au grids or 2.5 s for UltrAu grids, blot force of 3 (arbitrary
717 units), wait time of 5 s; chamber temperature of 6 °C, and relative humidity of 95%. Grids were plunge-
718 frozen in liquid ethane cooled by liquid nitrogen.
719

720 Cryo-EM data were collected in automated multi-hole mode on a 300 kV Titian Krios microscope for both
721 1-nt and 10-nt gapped DNA samples, controlled by SerialEM[67]. Micrographs were recorded at a nominal
722 magnification of 105,000× on a K3 direct electron detector (Gatan) operated in super-resolution counting
723 mode, with the objective lens underfocused in the range of 1.2–1.6 μm. For the 1-nt gapped DNA
724 sample, 111-frame movie stacks were recorded with a total exposure time of 3.4 s and a cumulative
725 electron dose of 49.6 $e^-/Å^2$. For the 10-nt gapped DNA sample, 50-frame movie stacks were recorded in
726 a total exposure time of 1 s and a cumulative dose of 59 $e^-/Å^2$. The calibrated physical pixel size at the
727 specimen level was 0.828 Å. Additional data collection parameters are summarized in **Tables S1** and
728 **S2**.
729
730 **Cryo-EM data processing**
731 Two cryo-EM datasets comprising 16,140 and 27,515 raw micrographs were collected for the DnaX-
732 complex–β-clamp bound to 1-nt gapped DNA and 10-nt gapped DNA, respectively. Image quality was
733 monitored during data collection using cryoSPARC Live v4.3.1 and v4.5.3[68] on a local workstation. Image
734 preprocessing—including patch motion correction (bin 2), contrast transfer function (CTF) estimation and
735 correction, blob-based particle picking (70–150 Å diameter), and particle extraction (bin 4)—were
736 performed concurrently. Following two-dimensional (2D) classification, particle displaying clear structural
737 features were selected and used to train a neural network–based particle picking model in Topaz[72]. After
738 further particle picking, 2D classification, and cleaning, selected particles were merged, and duplicate
739 particles with ≥40% overlap were removed such that only one particle was retained within ≤80 Å
740 distance (**Figures S1**, **S5**).
741
742 For the dataset containing 1-nt gapped DNA **(**16,140 micrographs), approximately 4.1 million particles
743 remained after duplicate removal and were subjected to ab initio 3D reconstruction followed by
744 heterogeneous refinement into four 3D classes. Two classes represented junk volumes and were
745 discarded, whereas the remaining two classes corresponded to two major clamp loading states, termed
746 state 1 and state 2, comprising ~1.8 and ~1.7 million particles, respectively. State 1 represents an initial
747 DNA recognition state, whereas state 2 corresponds to a post–DNA-entry state in which the 3′-dsDNA
748 has entered the β-clamp and the clamp gate is variably closed, accompanied by sharp bending of the 5′-
749 towards the 3′-dsDNA bound to the outer surface of the β-clamp (**Figure S1**).
750
751 After non-uniform refinement, the maps and associated particles were transferred to RELION 5.0.0 for
752 3D classification without alignment, followed by focused 3D classification on the DNA region using a
753 mask defined by a red dashed oval shape. Selected classes were then transferred back to cryoSPARC
754 v4.5.3 for global and local CTF refinement to correct aberrations introduced by UltrAu grids, followed by
755 reference-based motion correction and additional non-uniform and local refinement.

Three conformers were resolved for state 1: conformer 1 at 3.14 Å resolution with 105,100 particles (~6% of the population), in which 9 bp of the 20-bp 5′-dsDNA were ordered at the loader shoulder; conformer 2 at 2.71 Å resolution with 228,387 particles, with 5 bp of the 5′-dsDNA ordered; and conformer 3 at 2.73 Å resolution with 232,057 particles, in which the 5′-dsDNA was fully disordered (**Figures 1** and **S1**). Two conformers were obtained for state 2: conformer 1 at 2.72 Å resolution with 283,092 particles, in which the 3′-dsDNA had entered the β-clamp and the 5′-dsDNA bound the basic patch on the fully open clamp; and conformer 2 at 3.12 Å resolution with 203,554 particles, in which the 3′-dsDNA had progressed further into the clamp, the 5′-dsDNA had dissociated, and the β-clamp gate was narrowed by ~7 Å relative to conformer 1 (**Figures 2** and **S1**). To enhance the map interpretability, EMReady v2.2.1 was applied to the final maps of all five conformers[79,80].

For the dataset containing 10-nt gapped DNA (27,515 micrographs), approximately 8.5 million particles were used for ab initio 3D reconstruction, followed by heterogeneous refinement into three classes in cryoSPARC. The first class lacked discernible structural feature and was discarded. The second class, containing ~3.1 million particles, corresponded to the DnaX-complex alone and was subjected to two additional rounds of 2D classification. Selected particles were further refined by heterogeneous refinement using three copies of the initial map as references. One resulting class containing 478,123 particles exhibited the best structural features and was further refined by reference-based motion correction and non-uniform refinement to yield a final map at 2.95 Å resolution (**Figure S5**).

The third initial class, comprising ~4.7 million particles, corresponded to the ternary DnaX-complex–β-clamp–10-nt gapped DNA complex. This class underwent an additional round of heterogeneous refinement using eight copies of the initial map as references. Of the resulting eight classes, four were discarded due to low resolution (4–7 Å). The remaining four classes, resolved at 3.38–3.57 Å, represented distinct clamp loading intermediates: (1) a DNA gap recognition state in which the 3′-dsDNA had entered the loader chamber but its blunt end remained outside the β-clamp; (2) a state in which the 3′-dsDNA occupied both the loader and clamp chambers with the clamp gate fully open; (3-4) states in which the β-clamp gate was fully closed but exhibited variable flexibility.

Following additional 3D classification, merging of similar classes, reference-based motion correction, and non-uniform refinement, seven conformers of the DnaX-complex–β-clamp–10-nt gapped DNA were obtained: conformer 1 with 473,295 particles at 2.54 Å resolution (DNA recognition state); conformer 2 with 502,506 particles at 2.54 Å resolution (fully open, DNA unsettled); conformer 3 with 499,551 particles at 2.53 Å resolution (fully open, DNA settled); conformer 4 with 476,182 particles at 2.60 Å resolution (partially closed); and conformers 5–7 with 360,948, 539,340, 443,597 particles at 2.88, 2.60

792 and 2.70 Å resolution, respectively, in which the β-clamp gate was fully closed but the interfaces
793 between DnaX-complex and β-clamp varied (**Figure S5**).
794
795 The clamp loader used for cryo-EM analysis was the DnaX-holo-complex containing both ψ and χ
796 subunits. These subunits are small (137 and 147 amino acids; 15.2 and 16.6 kDa, respectively). and
797 diffuse density corresponding to χψ was observed near the expected binding site in some 2D class
798 averages. To improve visualization of this region, all χψ-containing particles (~7.8 million) from datasets
799 containing the loader alone and the loader bound to β-clamp and 10-nt gapped DNA were combined
800 after heterogeneous refinement and converted to RELION 5.0.0[81] using PyEM[82]. Focused 3D
801 classification without alignment was performed using a mask surrounding the χψ density. One class
802 containing 242,505 particles at 7.10 Å resolution exhibited clear density for the χψ heterodimer and was
803 transferred back to cryoSPARC for local refinement, yielding a map at 5.50 Å resolution (**Figure S5**).
804 This refined map was merged with the DNA gap recognition state map to generate a composite structure
805 of the χψ-containing DnaX-holo-complex engaged in β-clamp loading onto 10-nt gapped DNA.
806
807 **Model building, refinement, and validation**
808 Crystal structures of the γ-complex (PDB 1JR3)[7], the β-clamp–DNA complex (PDB 3BEP)[83], and SSB
809 peptide–bound χ–ψ subcomplex (PDB 3SXU)[36] were docked into the composite cryo-EM map of the
810 DnaX-holo-complex bound to β-clamp and 10-nt gapped DNA at the first loading state (DNA gap
811 recognition). The docked components were merged into a single model using ChimeraX[75] and served as
812 the initial model for subsequent refinement. The automated *de novo* model-building program
813 ModelAngelo[84] was also used to facilitate model construction.
814
815 Following manual refinement in COOT[76], the model was subjected to real space refinement in PHENIX[77],
816 followed by two additional rounds of iterative refinement between PHENIX and COOT. ISOLDE, a
817 molecular-dynamics-based flexible fitting-based plugin within ChimeraX, was then used to minimize
818 model clashes and improve local geometry. The final model was validated using the MolProbity program
819 as implemented in PHENIX[85].
820
821 This refined model was subsequently used as the starting model for building atomic models
822 corresponding to the five loading conformers with 1-nt gapped DNA and the seven loading conformers
823 with 10-nt gapped DNA. In regions of weaker densities, such as near the open gate of the β-clamp, the
824 model was rigid-body docked, followed by manual adjustment in COOT and final real space refinement in
825 PHENIX. All models were refined using the same procedure. Statistics for model refinement and
826 validation are provided in **Tables S1 and S2**. Structural panels were prepared using ChimeraX[86] and
827 assembled into figures in Adobe Illustrator (Adobe Inc, San Jose, CA).

828

829 **Fluorescence polarization–based DNA binding assay**

830 The affinity of the γ-complex for DNA was measured using either a tailed DNA substrate
831 (primer/template, p/T) or gapped DNA substrates containing 10- or 30-nt gaps, at a constant DNA
832 concentration of 10 nM. Importantly, γ-complex was used instead of τ-complex, since τ has a non-
833 specific DNA binding affinity for ssDNA and dsDNA. DNA oligonucleotides were gel purified prior to use.
834 DNA substrates were generated by annealing a 3′ Cy3-labelled Primer 1 either to a 50-nt template (p/T
835 DNA), to Primer 2 plus a 50-nt template (10-nt gapped DNA), or to Primer 2 plus 70-nt template (30-nt
836 gaped DNA) (**Figure 6B**), The annealed substrates were purified on a 10% native polyacrylamide gel.
837 Corresponding gel bands were excised, and DNA was extracted in TE buffer (10 mM Tris-HCl, pH 7.5, 1
838 mM EDTA), followed by concentration and buffer exchange into TE.

839

840 Fluorescence polarization–based binding assays were performed by titrating the γ-complex from 0 to 600
841 nM into reactions into 50-μL reactions containing 20 mM Tris-HCl (pH 7.5), 40 mM NaCl, 8 mM $MgCl_2$, 1
842 mM TCEP, 0.1 mM EDTA, and 100 μM ATPγS. Reactions were assembled in a 384-well plate and
843 incubated at 23 °C for 20 min. Plates were centrifuged for 20 s to remove air bubbles, and fluorescence
844 signals were recorded using a Synergy Neo2 plate reader (Agilent, Sant Clara, CA), with excitation at
845 535 nm and collection of emission between 560 and 580 nm. Three independent experiments were
846 performed for each titration.

847

848 Relative fluorescence intensity (I/I_0) was plotted as a function of γ-complex concentration.
849 Apparent dissociation constants ($^{App}K_d$) were determined by fitting the data to a one-site binding model
850 using Origin Software (OriginLab, Northampton, MA).

851

852 **Measurement of clamp loading rate onto primed versus gapped DNA**

853 The rate of clamp loading was measured using a replication assay with Pol III αε complex, which
854 requires a loaded β-clamp to extend a primed DNA substrate (**Figures 6C** and **S8A**). In this assay, β-
855 clamp was loaded onto a 5′ ^{32}P-labeled primed site in the presence of γ-complex and Pol III αε complex,
856 and timed aliquots were removed for analysis by urea–PAGE. To ensure that clamp loading was the
857 rate-limiting step, Pol III was supplied in sufficient excess such that the distribution of reaction products
858 was determined by clamp loading rather than by the rate of primer extension. Under these conditions,
859 DNA products at all time points exhibit the same size distribution on urea–PAGE but increase in intensity
860 over time. As a control, reactions containing Pol III alone (lacking β-clamp and γ-complex) were
861 performed and showed no primer extension, as expected.

862

863 The DNA template (replication template) and the 5′ ^{32}P-labeled primer (replication primer 1) used in these
864 assays are listed in the **KEY RESOURCES TABLE**. For gapped DNA substrates, a second
865 oligonucleotide (replication primer 2) was annealed downstream of the 3′ terminus of the 5′ ^{32}P-labeled
866 replication primer 1 on a 45-nt template. The replication template strand contained biotin at both termini
867 to retain loaded clamps. For singly primed DNA substrates, replication primer 1 was labeled with ^{32}P
868 using T4 polynucleotide kinase (Sigma, St. Louis, MO) and annealed to the replication template. For the
869 45-nt gapped template, both the ^{32}P-labeled replication primer 1 and the unlabeled replication primer 2
870 were annealed to the replication template.
871
872 Reactions were assembled in a scaled-up volume (4.5×; 90 µL total) to allow removal of multiple timed
873 aliquots. Each reaction contained 0.9 pmol of ^{32}P-primed template and 5.3 pmol streptavidin tetramer in
874 Buffer B supplemented with 8 mM $MgCl_2$. Reactions were incubated at 23 ºC for 15 min, followed by
875 addition of 2.7 pmol SSB and incubation for an additional 5 min at 37 °C. Reactions were initiated by
876 addition of 0.9 pmol *E. coli* Pol III, 0.9 pmol β-clamp, and 0.9 pmol γ-complex in a final volume of 90 µL
877 buffer B containing 8 mM $MgCl_2$, 2 mM ATP, and 100 mM each of dATP, dCTP, dGTP and ^{32}P-dTTP.
878
879 Reactions were incubated at 23 ºC, and 20-µL aliquots were withdrawn at 0.5, 1, 2, and 5 min and
880 quenched with 25 µL stop solution (76% formamide, 14 mM EDTA, 0.02% bromophenol blue, 2% SDS).
881 Replicated products were resolved on a 15% urea–denaturing polyacrylamide gel (**Figure S8A**). Gels
882 were exposed to a storage phosphor screen and scanned using a Typhoon PhosphorImager (GE
883 Healthcare). Product bands were quantified using ImageQuant software (GE Healthcare). Each reaction
884 was performed in triplicate, and mean values and standard deviations were calculated using Microsoft
885 Excel.
886
887 **ATPase assays**
888 Two oligonucleotides (oligo 1: 5'-GGCTCGCTACGGCTATACGG-3'; oligo 2: 5'-
889 GATTCGTATCGCCTATACCG-3') were both annealed to a template oligo, 5'-
890 CGGTATAGGCGATACGAATC(T_n)CCGTATAGCCGTAGCGAGCC-3', where n = 0, 1, 2, 5, 10,
891 to generate DNA substrates containing a nick or 1-, 2-, 5- or 10-nt gaps. The resulting DNA substrates
892 were separated from unannealed oligonucleotides by native 20% agarose gel electrophoresis and
893 purified from the gel.
894
895 ATPase reactions were performed by mixing 50 nM wild-type γ-complex with 500 nM purified gapped
896 DNA substrates and 200 nM β-clamp in a total volume of 30 µL containing 20 mM Tris-HCl (pH7.5), 0.1
897 mM EDTA, 40 µg/mL BSA, 4% glycerol, 5 mM DTT, 8 mM $MgCl_2$, 0.5 mM ATP, and 55 nM γ-^{32}P-ATP.

898 Reactions were incubated at 37 °C, and 5-μL aliquots were removed at 5, 10, 20, and 30 min and
899 quenched with an equal volume of 0.5 M EDTA.
900
901 One microliter of each quenched reaction was spotted onto PEI Cellulose F thin-layer chromatography
902 (TLC) plate (Millipore Sigma) and developed in 0.75 M $KHPO_4$ (pH 4.4). TLC plates were exposed to a
903 PhosphorImager screen and scanned using an Amersham Typhoon instrument. Radioactive ATP and
904 inorganic phosphate were quantitated using ImageQuant software (**Figure S8B**).
905
906 **QUANTIFICATION AND STATISTICAL ANALYSIS**
907 Fluorescence polarization–based binding assays measuring γ-complex interactions with different DNA
908 substrates were performed in three independently performed experiments. Data fitting was carried out
909 using Origin Software (OriginLab, Northampton, MA), and results are presented as mean ± standard
910 error of the (SEM) in **Figure 6B**. Statistical analysis of cryo-EM structures was performed during model
911 refinement in Phenix, with details provided in **Tables S1** and **S2**.
912
913 **Supplemental video legends**
914
915 **Video 1. Overview of thirteen β-clamp loading intermediates captured for DnaX-complex loading**
916 **β-clamp onto either a 1-nt gapped DNA (five intermediates) or a 10-nt gapped DNA (eight**
917 **intermediates).** The thirteen atomic models are aligned and displayed individually, each rotated by 360º
918 about the Y axis.
919
920 **Video 2. Morphing of β-clamp loading onto a 1-nt gapped DNA substrate.** The morph integrates
921 previously reported structures of DnaX-complex loading β-clamp onto tailed DNA[16,17], with the five
922 loading intermediates captured here using a 1-nt gapped DNA. The animation begins with formation of a
923 binary DnaX-complex–β-clamp complex in the presence of ATP, which induces β-clamp gate opening.
924 The open clamp then engages the 3'-dsDNA segment of the 1-nt gapped DNA via a conserved basic
925 patch on the outer surface of the β-clamp near the open gate. This interaction is followed by sharp
926 bending of the 5′-dsDNA towards the 3′-dsDNA, generating a stressed U-shaped DNA conformation and
927 exposing the recessed 3′ end. The resulting DNA strain promotes insertion of the recessed 3′ end into
928 the DnaX-complex chamber, entry of the 3′-dsDNA into the β-clamp, and binding of the 5′-dsDNA to the
929 clamp basic patch vacated by the 3'-dsDNA. During this process, the δ-subunit Y316 sensor
930 recognizes—but does not unwind—the recessed DNA 3′ end. Subsequent DNA engagement within the
931 β-clamp chamber is proposed to drive clamp gate closure via electrostatic interactions, stimulate ATP
932 hydrolysis, and trigger dissociation of the DnaX-complex, completing the clamp loading reaction.
933

934 **Video 3. Morphing of β-clamp loading onto a larger gapped DNA (>6 nt).** The animation was
935 generated in ChimeraX based on the reported structures of the β-clamp (PDB: 1MMI)[87], the *E. coli* DnaX-
936 complex bound to β-clamp in the absence of DNA (PDB: 8GIY and 7TI8)[16,17], and the eight loading
937 intermediates captured here with a 10-nt gapped DNA. In the presence of ATP, the DnaX-complex binds
938 and opens the β-clamp gate. Because the recessed DNA 3′ end is accessible in large-gapped
939 substrates, it can directly enter the clamp loader chamber and engage the δ-subunit Y316 sensor
940 residue, while the 3′-dsDNA binds to the basic patch on the exterior surface of β-clamp. Electrostatic
941 attraction between the negatively charged DNA backbone and the positively charged interior of the β-
942 clamp promotes insertion of the 3′-dsDNA into the clamp chamber and drives clamp gate closure,
943 ultimately leading to dissociation of the DnaX-complex and formation of a DNA-encircling β-clamp.
944
945

946 **Figures and legends**

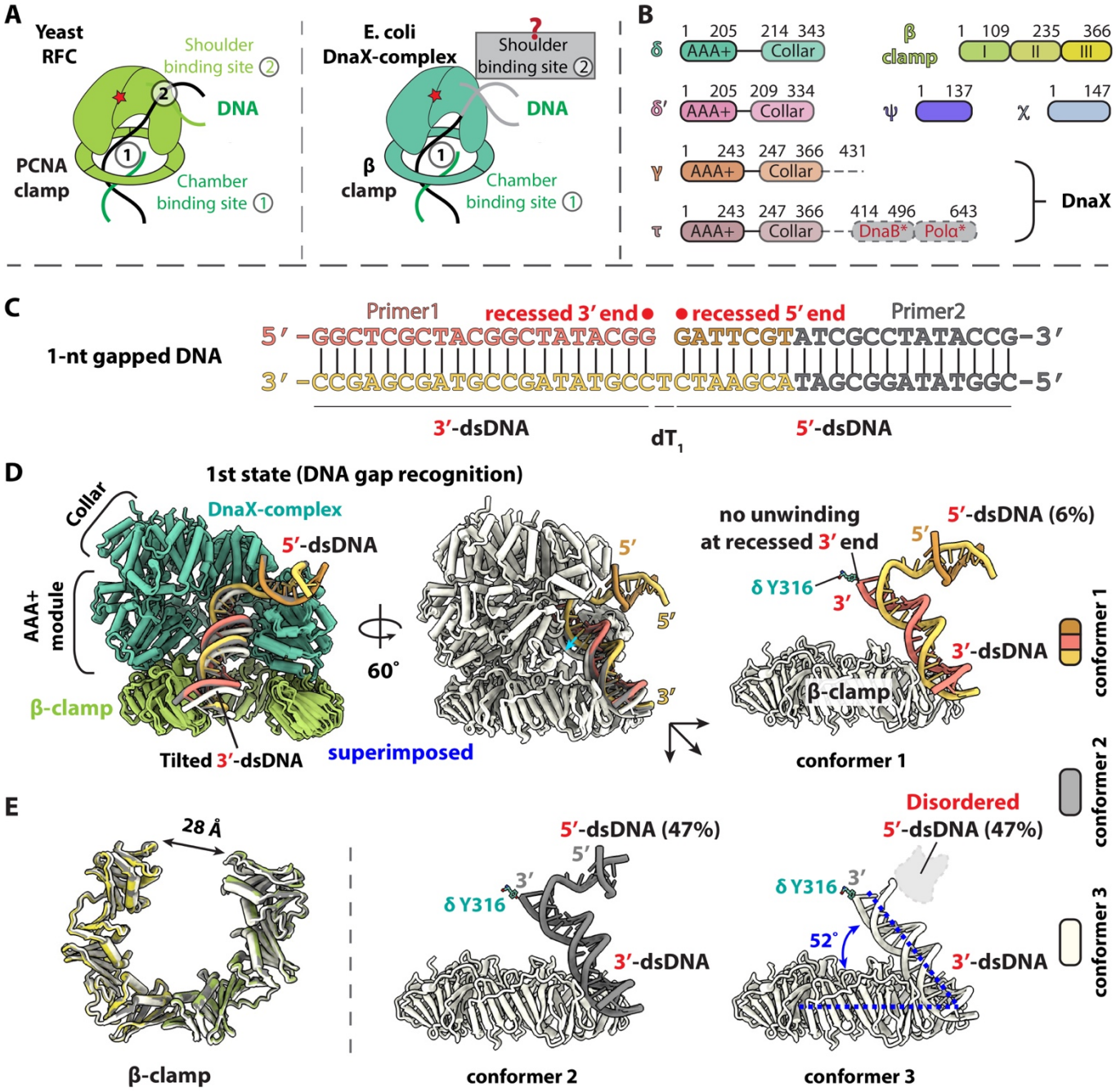

947

948 **Figure 1. The *E. coli* DnaX-complex loading β-clamp onto nicked or 1-nt gapped DNA.** (**A**)
949 Schematic illustrating that eukaryotic RFC uses a shoulder DNA-binding site to facilitate PCNA loading
950 onto small-gaped DNA. In contrast, how the bacterial DnaX-complex loads the β-clamp onto nicked or
951 small gapped DNA, and whether it possesses a functional shoulder DNA-binding site, has remained
952 unclear. (**B**) Domain organizations of the DnaX-holo-complex and the β-clamp. The *E. coli dnaX* gene
953 encodes the full-length τ subunit and a C-terminally truncated γ subunit lacking the C-terminal domain
954 (CTD). The mobile τ CTD (grey) contains regions that interact with DnaB helicase and Pol III α
955 (asterisks). (**C**) Sequence of the 1-nt gapped DNA substrate used for cryo-EM study. The unresolved
956 region is shown in gray. The duplex DNA segment containing the recessed 3′ end is referred to as the 3′-

957 dsDNA, and the duplex segment containing the recessed 5′ end is referred to as the 5′-dsDNA. (**D**) Three
958 conformers of the first major loading state—the DNA recognition state—of the DnaX-complex–β-clamp
959 bound to 1-nt gapped DNA. The top two panels show two views of the three superimposed conformers.
960 In all conformers, the recessed DNA 3′ end has entered the clamp loader chamber, whereas the 3′-
961 dsDNA remains outside the β-clamp. The 5′-dsDNA is partially ordered in conformer 1 (7 bp) and
962 conformer 2 (5 bp) but is completely disordered in conformer 3 (bottom panels). Notably, no base pair
963 separation is observed at the recessed 3′ end, indicating that the δ-subunit Y316 does not unwind DNA
964 (lower left panel). (**E**) Superposition of the β-clamps from the three conformers showing the identical gate
965 opening of ~28 Å. Unless otherwise indicated, distance measurements were performed using surface
966 representation in ChimeraX[75].
967

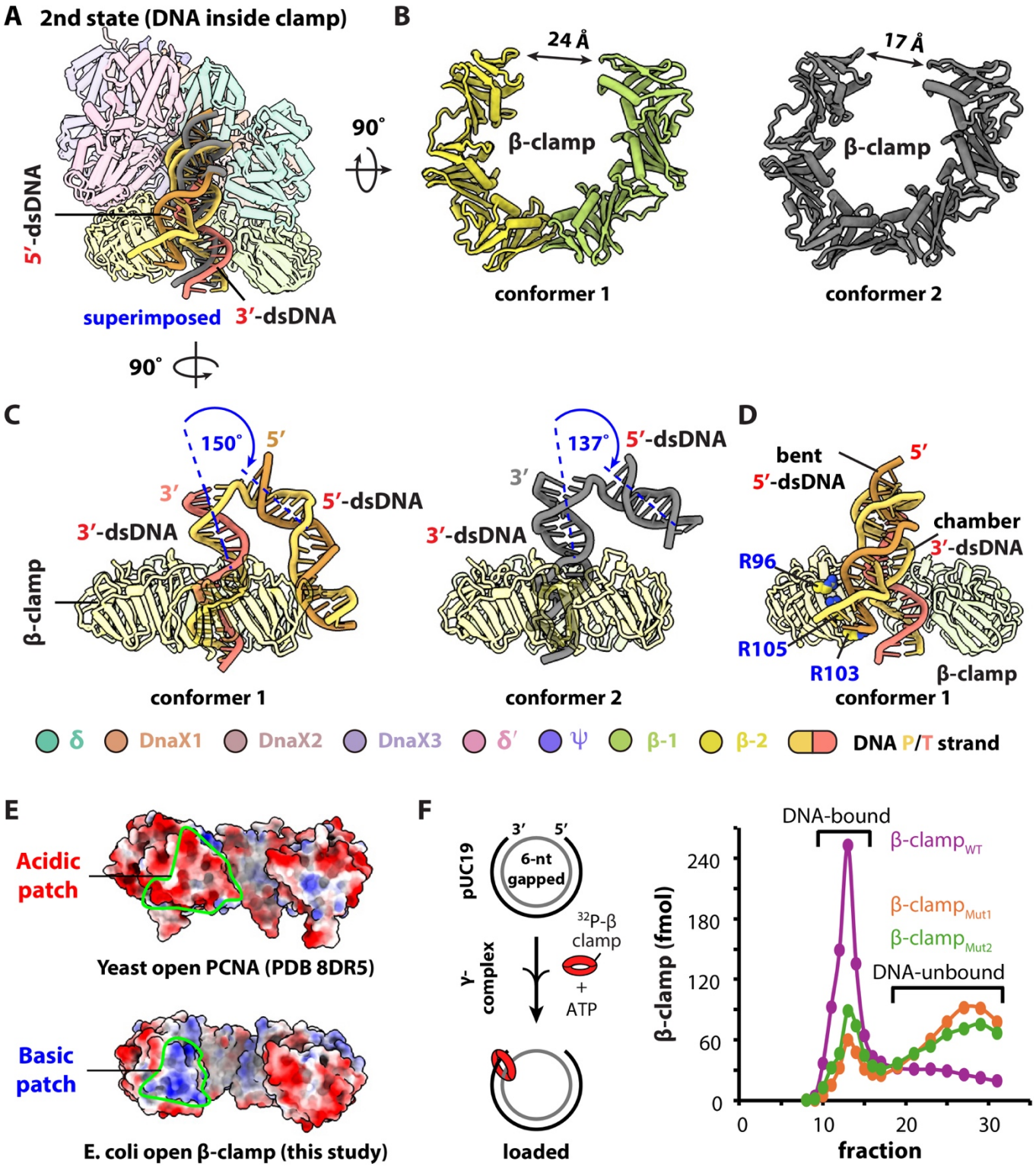

Figure 2. The second loading state of the DnaX-complex during β-clamp loading onto 1-nt gapped DNA and the role of a β-clamp basic patch. (**A**) Superimposition of conformers 1 (color) and 2 (gray) of the second major loading state, in which the 3′-dsDNA has entered the β-clamp chamber. (**B**) Side-by-side comparison of the β-clamp in conformers 1 and 2, highlighting differences in clamp gate width. (**C**) Side view of the superimposed structures in (A), with the DnaX-complex omitted for clarity. The two

975 conformers are shown separately. In conformer 1, the 5′-dsDNA bends sharply and binds the outer
976 surface of the β-clamp at the site previously occupied by the 3′-dsDNA. In conformer 2, 5′-dsDNA
977 dissociates from the β-clamp and becomes partially flexible (11 bp ordered), concomitant with further
978 clamp closure. (**D**) Three positively charged residues (R96, R103, and R105) form a distinct basic patch
979 on the outer surface of the β-clamp near the left gate. (**E**) Comparison of this region with yeast PCNA
980 reveals that the corresponding surface is acidic. (**F**) Substitution of the three arginine residues with
981 alanine (β-clamp$_{Mut1}$) or glutamate (β-clamp$_{Mut2}$) reduced β-clamp loading efficiency onto a 6-nt gapped
982 pUC19 plasmid DNA to approximately one-third of that observed with wild-type β-clamp (β-clamp$_{WT}$). In
983 panels (**A)**, (**C**), and (**D**), protein components are shown as 80% transparent cartoons for clarity.
984

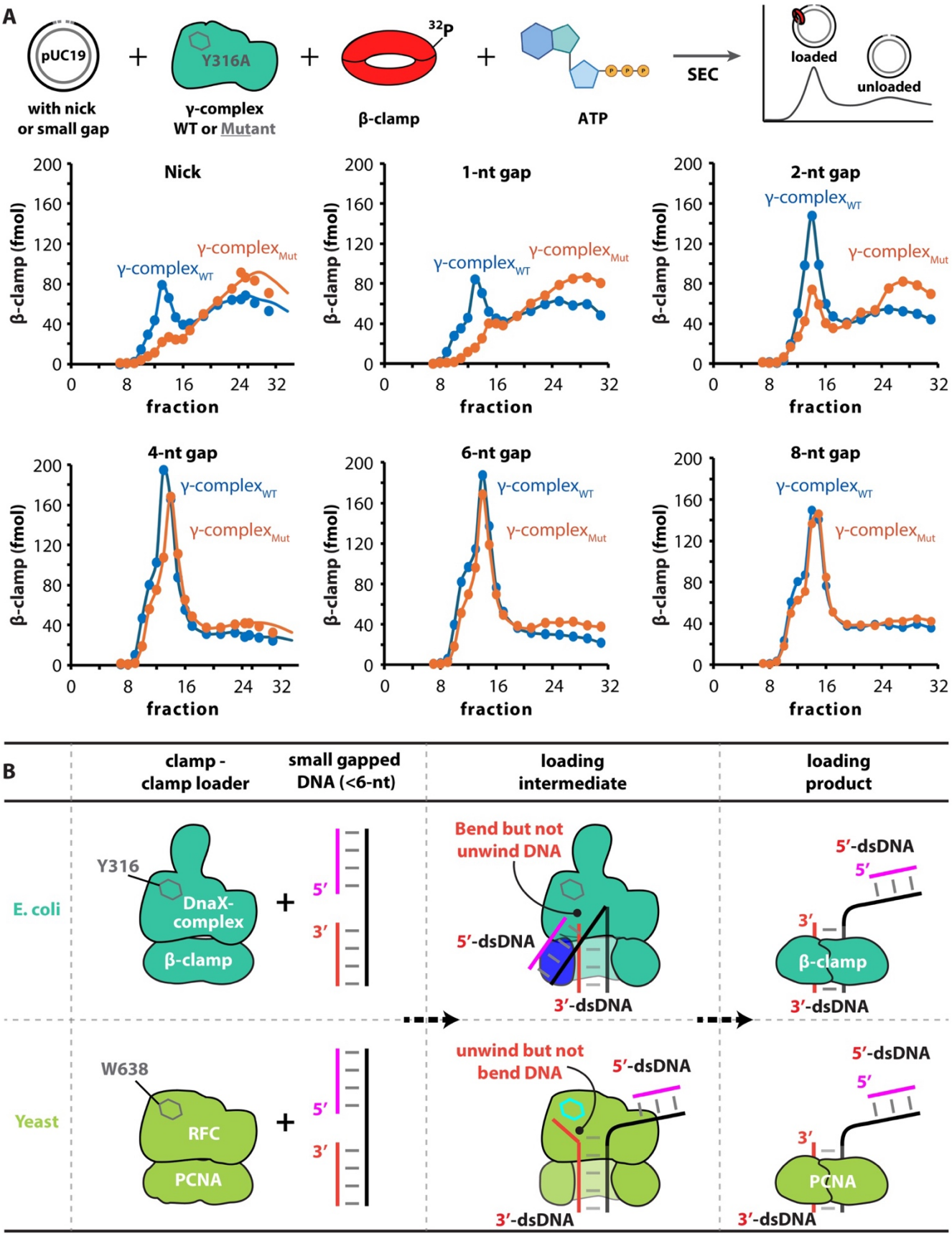

Figure 3. The *E. coli* DnaX-complex employs a DNA-bending strategy to load the β-clamp onto DNA containing small gaps (<6 nt). (**A**) Comparison of β-clamp loading efficiencies mediated by the

988 wild-type clamp loader (γ-complex$_{WT}$) and a separation-pin mutant harboring the δ-subunit Y316A
989 substitution (γ-complex$_{Mut}$) using plasmid DNA substrates containing a nick or gaps of defined sizes**.**
990 From the γ-complex$_{Mut}$, loading efficiency increases progressively with gap size, approaching that of the
991 wild-type complex, reaching ~85% efficiency on 4-nt gapped DNA and ~90% on 6-nt gapped DNA (see
992 **Methods** for details). (**B**) Schematic comparison of clamp loading mechanisms in bacteria (e.g., *E. coli*)
993 and eukaryotes (e.g., *S. cerevisiae*) at nicked or small gapped DNA. In yeast, the Rfc1 separation pin
994 residue W638 unwinds up to ~6 bp at the recessed 3′ end to generate a sufficiently long gap for PCNA
995 loading[14,15]. In contrast, the corresponding residue in *E. coli*, δ Y316, recognizes the recessed DNA 3′
996 end without unwinding DNA. Instead, the bacterial DnaX-complex, but not RFC, induces sharp DNA
997 bending (~150°) to enable clamp loading.
998

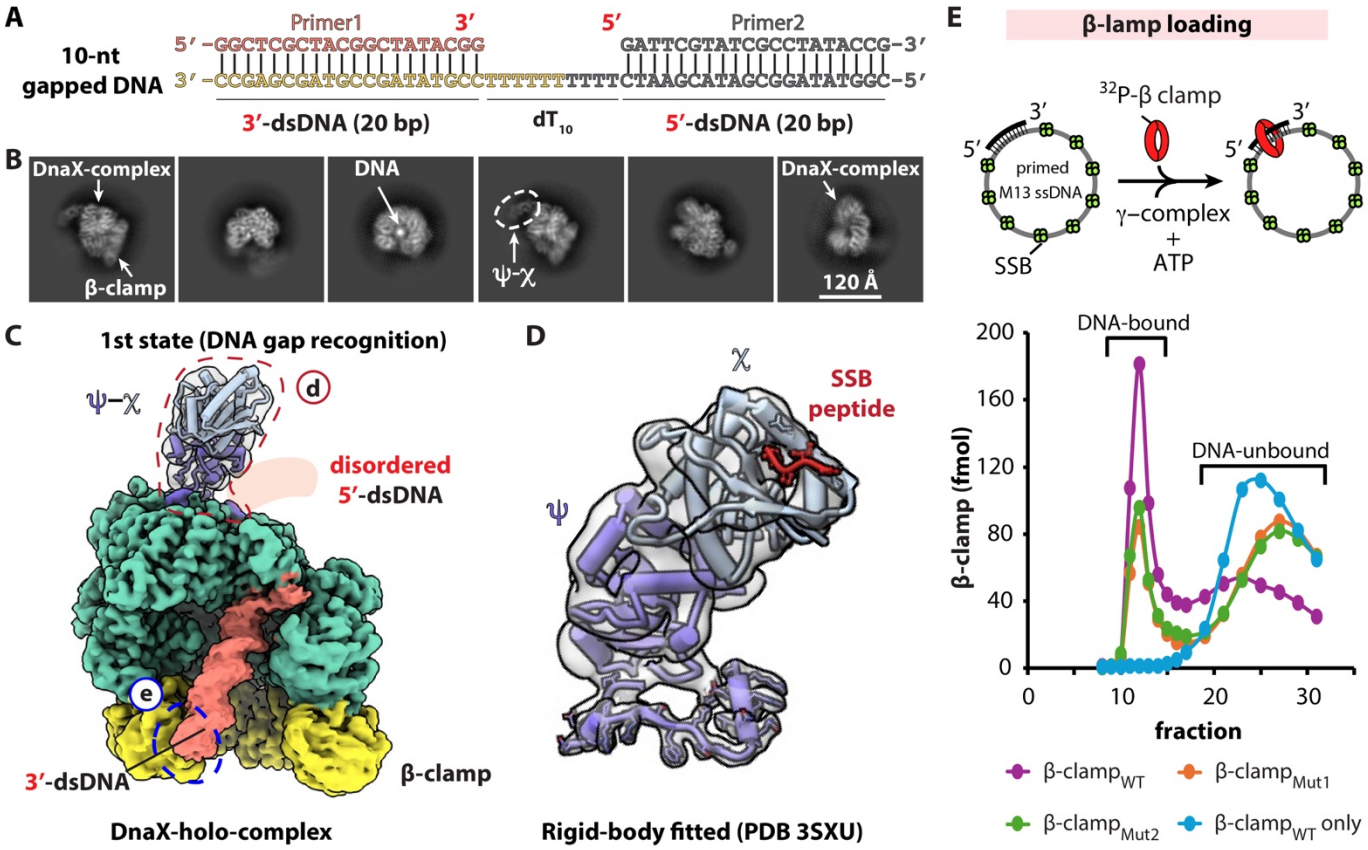

Figure 4. β-clamp loading by the DnaX-holo-complex onto a 10-nt gapped DNA substrate. (**A**) Architecture of the 10-nt gapped DNA used for cryo-EM analysis. (**B**) Representative 2D class averages of clamp loading intermediates. The dashed oval indicates weak density corresponding to the χψ heterodimer. (**C-D**) Front views of a DnaX-holo-complex in the 1st DNA gap recognition state during loading of the β-clamp onto a 10-nt gapped DNA. In this state, the 5′-dsDNA is disordered, whereas the 3′-dsDNA is ordered and bind to the outer surface of the β-clamp. The region outlined by the red dashed line (C) is enlarged in (**D**), showing a rigid-body docked χψ crystal structure bound to a SSB peptide[36]. The 3′-dsDNA is observed to bind the β-clamp basic patch (blue dashed outline), similar to that observed with 1-nt gapped DNA. (**E**) Loading efficiency of the β-clamp basic patch mutants on a singly primed DNA with a larger gap size. β-clamp$_{Mut1}$ and β-clamp$_{Mut2}$ harbor R96, R103, and R105 substitutions to alanine or glutamate, respectively, and were ^{32}P-labelled for quantification alongside wild-type β-clamp (β-clamp$_{WT}$).

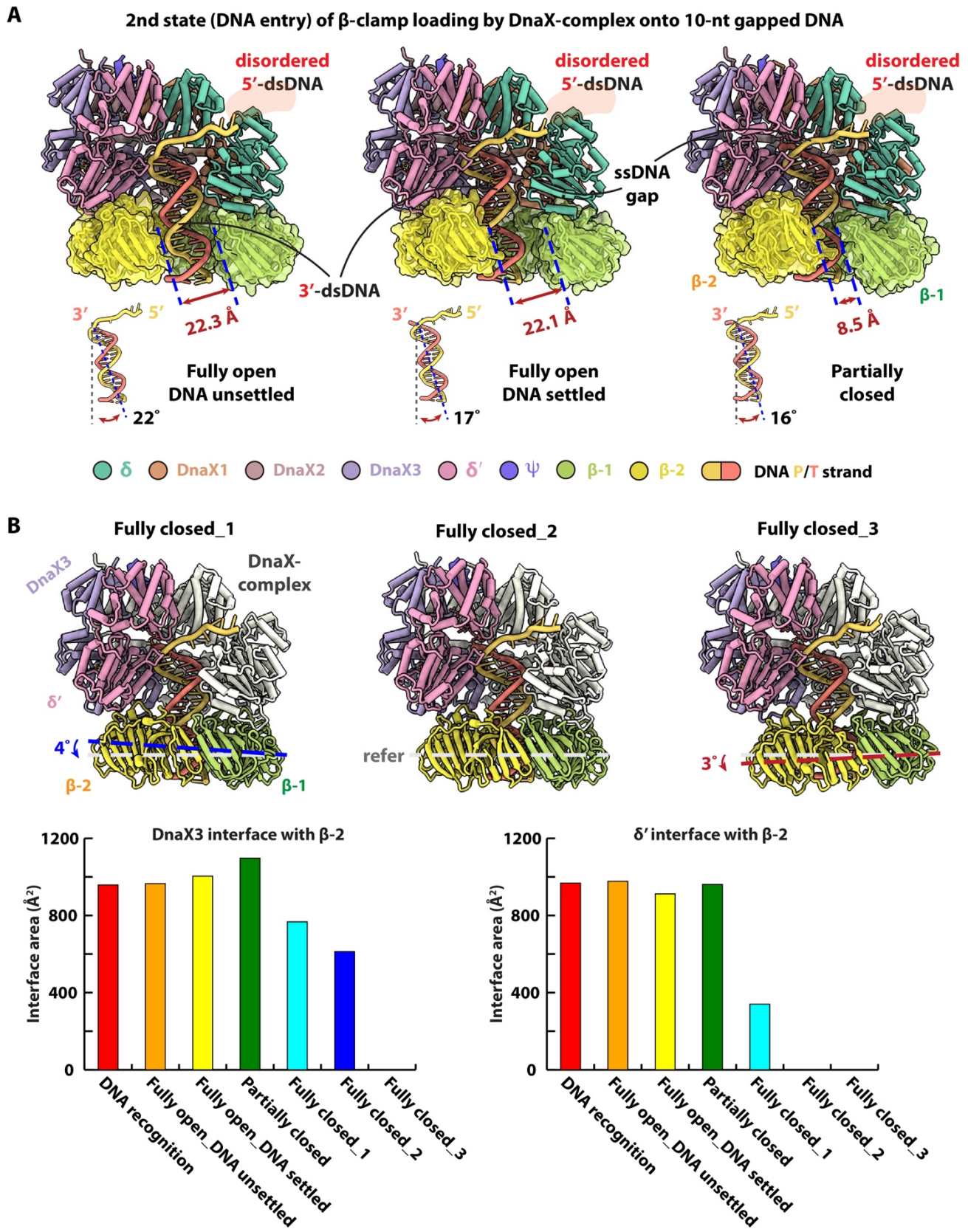

Figure 5. Six conformers in the second loading state of the DnaX-complex during β-clamp loading onto a 10-nt gapped DNA substrate. (**A**) In conformers 1–3, progressive settling of the 3′-dsDNA into the β-clamp is accompanied by a reduction in DNA tilt from 22° to 17° to 16°. Concurrently, the β-clamp

1018 gate narrows from 22.3 Å to 22.1 Å and then to 8.5 Å, illustrating stepwise clamp closure. (**B**) In
1019 conformers 4–6, in which the β-clamp gate is fully closed, the β-clamp progressively dissociates from the
1020 clamp loader, as indicated by clamp tilting away from the loader by ~4° and an additional ~3°,
1021 respectively. The lower panels show the corresponding interface areas between the DnaX3 and β2
1022 subunits (left) and between δ′ and β2 subunits (right), highlighting changes in protein-protein interactions
1023 during clamp loader release.
1024

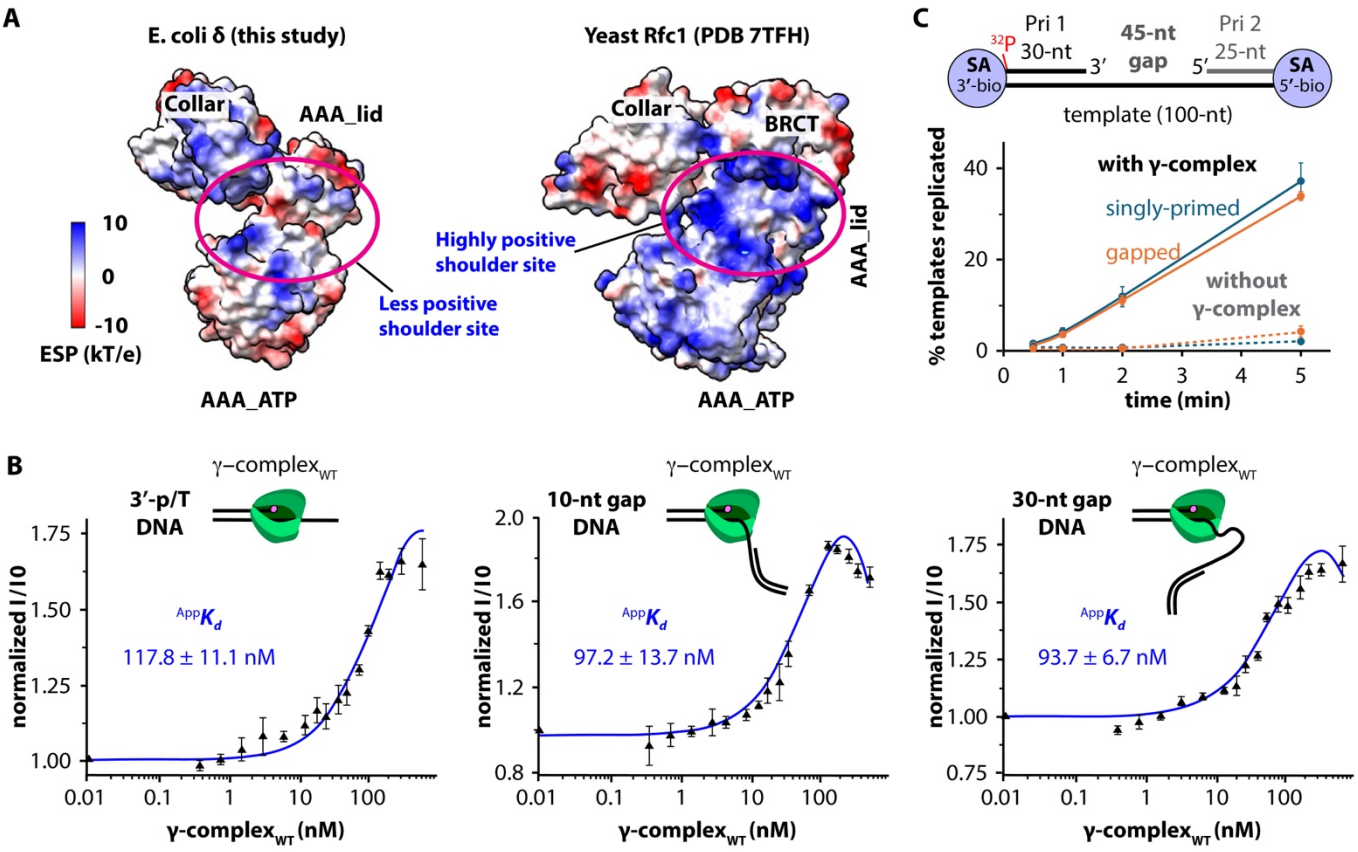

Figure 6. The DnaX-complex shoulder is not highly positively charged and is not required for efficient clamp loading. (**A**) Comparison of electrostatic surface potentials showing that the eukaryotic clamp loader subunit Rfc1 (PDB: 7TFH) contains a highly positively charged dsDNA binding site at the shoulder region (purple oval), whereas the corresponding region of *E. coli* δ (this study) lacks a comparably charged surface. (**B**) Fluorescence anisotropy measurements indicate that the presence of a 5′-dsDNA does not significantly enhance DNA binding by the DnaX-complex. DNA substrates consisting of a tailed primer/template with only a recessed 3′ end (left), a 10-nt gapped DNA (middle), or a 30-nt gapped DNA (right) bind the DnaX-complex with similar apparent affinities ($^{App}K_d$ values of 118 nM, 97 nM, and 94 nM, respectively). Fluorescence signals were normalized (I /I0) to the signal obtained in the absence of protein. Assays were performed in triplicate, and $^{App}K_d$ values are shown as mean values (black triangles) ± standard deviations (error bars). (**C**) The rate of β-clamp loading onto a DNA containing only a recessed 3′ end is comparable to that observed for loading onto a 45-nt gapped DNA containing both recessed 3′ and 5′ ends.

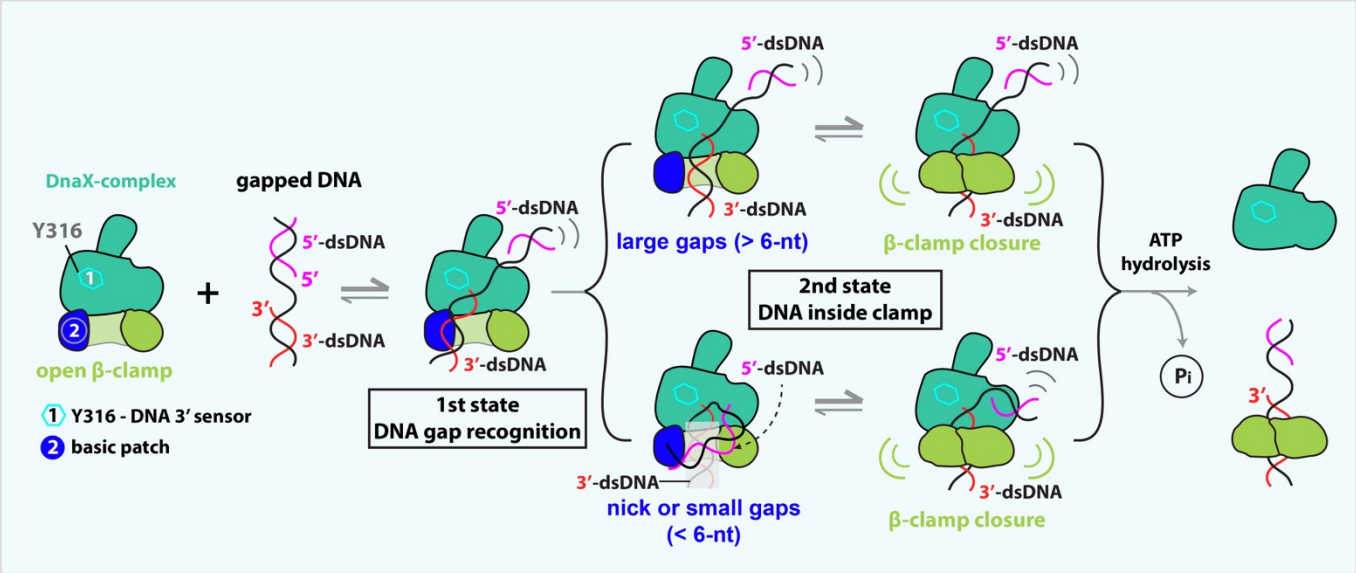

Figure 7. Proposed DNA structure–dependent mechanism for β-clamp loading by the DnaX-complex. The bacterial clamp loader recognizes, but does not unwind, the recessed DNA 3′ end via the δ-subunit Y316 residue, and the β-clamp contains a conserved basic patch on its outer surface that can bind dsDNA. When a gapped DNA substrate encounters a DnaX-complex bound to an open β-clamp, the 3′-dsDNA binds the β-clamp basic patch in a tilted orientation (first state). If the ssDNA gap is sufficiently long to thread through the clamp loader (>6 nt), the 5′-dsDNA remains outside the loader while the 3′-dsDNA diffuses to the higher affinity interior chamber of the β-clamp (second state). In contrast, at a nick or a small ssDNA gap (<6 nt), the adjacent 5′-dsDNA bends sharply toward the 3′-dsDNA, adopts a U-shaped conformation that promotes displacement of the 3′-dsDNA toward the β-clamp chamber. Once the 3′-dsDNA enters the clamp interior, electrostatic interactions between the negatively charged DNA backbone and the positively charged inner surface of the β-clamp are proposed to drive clamp gate closure. Subsequent ATP hydrolysis triggers dissociation of the DnaX-complex, leaving the β-clamp encircling the 3′-dsDNA.

1055 **Table S1. Cryo-EM data collection, refinement, and atomic model validation**
1056

Structures	DnaX-complex–β-clamp–1-nt gapped DNA					DnaX-complex[a]	ψ-χ focus refined[a]
	State 1 conf. 1	State 1 conf. 2	State 1 conf. 3	State 2 conf. 1	State 2 conf. 2		
EMDB ID	EMD-71013	EMD-71014	EMD-71015	EMD-71016	EMD-71017	EMD-71018	EMD-71020
PDB ID	9OYB	9OYC	9OYD	9OYE	9OYF	9OYG	
Data collection							
Magnification	105,000						
Voltage (kV)	300						
Dose ($e^-/Å^2$)	49.6					59	
Under-focus (μm)	1.2 - 1.6						
Pixel size (Å)	0.828						
Symmetry	C1						
Initial particle #	4.1 million					3.1 M	7.8 M
Final particle #	105,100	228,387	232,057	283,092	203,554	478,123	242,505
Map resolution (Å)	3.14	2.71	2.73	2.72	3.12	2.95	5.50
FSC threshold						0.143	
Map resolution range (Å)	2.7 – 11.0	2.4 – 11.0	2.3 – 12.0	2.4 – 10.3	2.7 – 10.1	2.5 – 9.5	4.5 – 13.0
Refinement							
Initial model used (PDB code)	1JR3, 3BEP					1JR3	3SXU
Map sharpening B factor ($Å^2$)	-105.2	-86.9	-87.1	-99.5	-107.2	-116.7	-211.4
Map to model CC_{mask}	0.89	0.89	0.88	0.88	0.88	0.79	
Model composition							
Non-hydrogen atoms	21,074	20,894	20,661	21,517	21,127	14,125	
Protein and DNA residues	2,532; 59	2,530; 51	2,529; 40	2,531; 81	2,531; 62	1794; 0	
Ligands	10	10	10	10	10	10	
R.m.s. deviations							
Bond lengths (Å)	0.004	0.004	0.003	0.006	0.005	0.003	
Bond angels (°)	0.756	0.631	0.594	0.684	0.669	0.623	
Validation							
MolProbity score	1.34	1.67	1.26	1.38	1.49	1.58	
Clashscore	5.53	4.56	4.99	6.08	5.47	8.42	
Poor rotamers (%)	0	0	0	0	0	0	
Ramachandran plot							
Favored (%)	97.81	98.33	98.29	97.77	96.86	97.35	
Allowed (%)	2.19	1.67	1.71	2.23	3.14	2.65	
Disallowed (%)	0	0	0	0	0	0	

1057 [a]: The last two columns are from dataset with 10-nt gapped DNA (continued in **Table S2**).

1058 **Table S2. Cryo-EM data collection, refinement, and atomic model validation**
1059

Structures	DnaX-complex–β-clamp–10-nt gapped DNA						
	DNA recognition	**fully open, DNA unsettled**	**fully open, DNA settled**	**partially closed**	**fully closed 1**	**fully closed 2**	**fully closed 3**
EMDB ID	EMD-71021	EMD-71022	EMD-71023	EMD-71024	EMD-71025	EMD-71026	EMD-71027
PDB ID	9OYH	9OYI	9OYJ	9OYK	9OYL	9OYM	9OYN
Data collection and processing							
Magnification	105,000						
Voltage (kV)	300						
Electron dose (e^-/Å^2)	59						
Under-focus range (μm)	1.2 - 1.6						
Pixel size (Å)	0.828						
Symmetry imposed	C1						
Initial particle images (no.)	8,537,193						
Final particle images (no.)	473,295	502,506	499,551	476,182	360,948	539,340	443,597
Map resolution (Å)	2.54	2.54	2.53	2.60	2.88	2.60	2.70
FSC threshold	0.143						
Map resolution range (Å)	2.2 – 9.5	2.2 – 9.3	2.2 – 9.5	2.3 – 9.6	1.8 – 9.9	2.3 – 9.4	2.4 – 9.9
Refinement							
Initial model used (PDB code)	1JR3, 3BEP, 3SXU						
Map sharpening B factor (Å^2)	-91.6	-92.5	-92.6	-95.7	-99.1	-98.1	-99.0
Map to model CC_{mask}	0.71	0.87	0.75	0.87	0.75	0.86	0.82
Model composition							
Non-hydrogen atoms	22,702	20,796	20,835	20,861	20,835	20,861	20,843
Protein and DNA residues	2,779; 44	2,531; 46	2,531; 47	2,534; 47	2,532; 47	2,534; 47	2532; 47
Ligands	10	10	11	11	11	11	11
R.m.s. deviations							
Bond lengths (Å)	0.002	0.005	0.007	0.003	0.003	0.004	0.005
Bond angels (°)	0.480	0.634	0.687	0.530	0.489	0.587	0.579
Validation							
MolProbity score	1.40	1.21	1.52	1.24	1.45	1.21	1.37
Clashscore	7.29	4.31	6.67	4.73	6.98	4.25	5.19

Poor rotamers (%)	0	0	0	0	0	0	0
Ramachandran plot							
Favored (%)	98.15	98.17	97.13	98.13	97.69	98.57	97.54
Allowed (%)	1.85	1.83	2.87	1.87	2.31	1.43	2.46
Disallowed (%)	0	0	0	0	0	0	0

1060

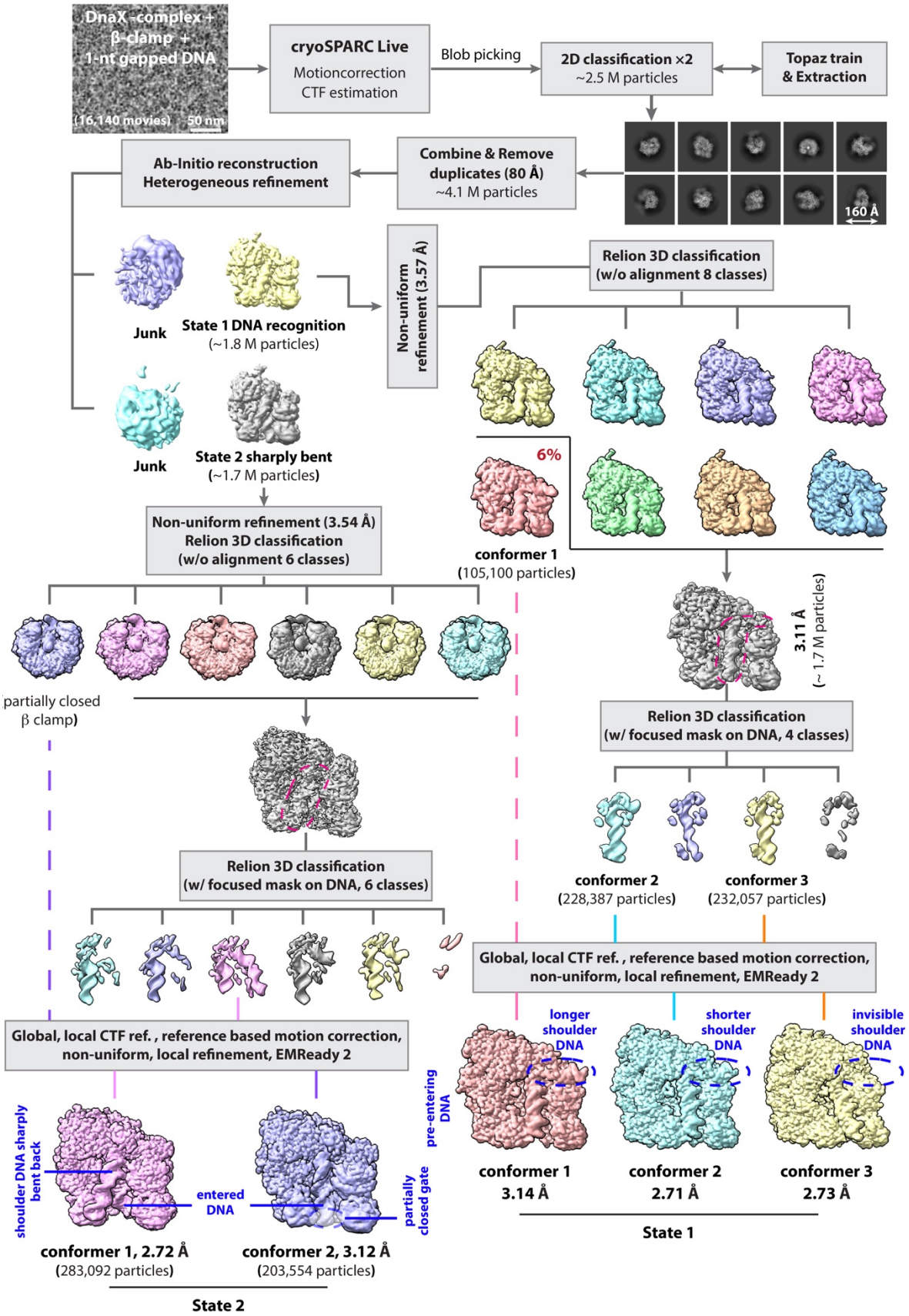

Figure S1. Cryo-EM data processing of the DnaX-complex–β-clamp bound to 1-nt gapped DNA. A representative micrograph from approximately 16,000 movies collected on a 300 kV Titan Krios

microscope is shown, with scale bar indicated. Image processing was performed using cryoSPARC v4.5 and Relion v5.0[68,88]. Two major clamp loading states were identified: a first state comprising three conformers and a second state comprising two conformers.

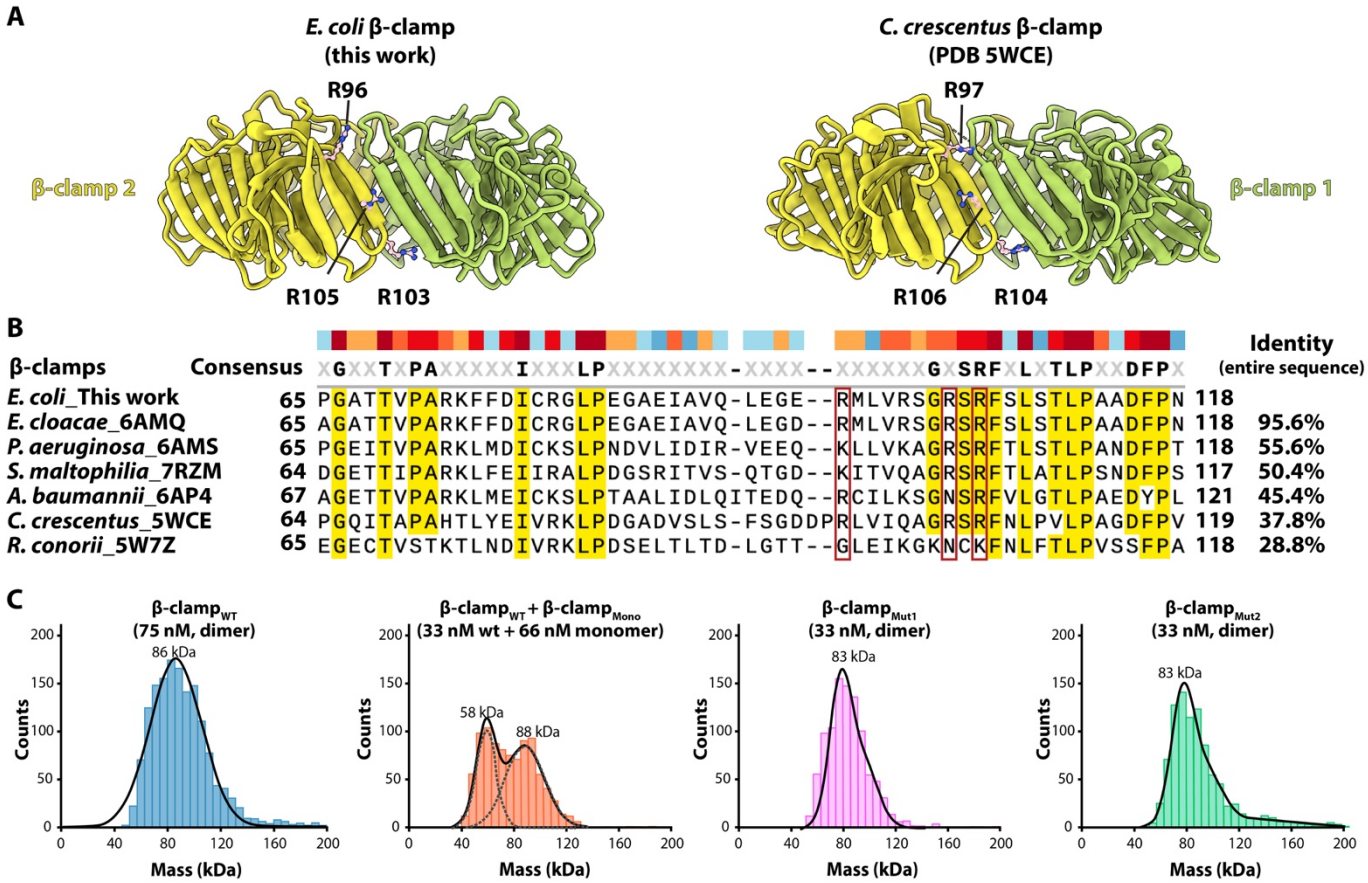

Figure S2. The basic patch on the outer surface of the β-clamp is conserved among prokaryotes. Related to Figure 3. (**A**) Structural comparison of the *E. coli* β-clamp with that of *Caulobacter crescentus* as a representative example. The three positively charged residues that form the conserved basic patch are shown as sticks and are located on the outer surface near the left side of the DNA entry gate between the two β subunits. (**B**) Structure-based sequence alignment of the β-clamp region containing the three basic residues, highlighted by red boxes. Structures were aligned using ChimeraX[86], and PDB accession code for each structure is listed following the species name. (**C**) The β-clamp mutants used in this study remain dimeric in solution. Mass photometry measurements have a low molecular weight detection limit of ~40 kDa; therefore, apparent β monomer mass values are expected to be slightly higher than theoretical monomer mass. As controls, wild-type β-clamp dimers and a previously characterized β monomer mutant, in which the hydrophobic core residues were mutated to disrupt dimerization (I272A/L273/A)[89] were analyzed. Both β-clamp$_{Mut1}$ and β-clamp$_{Mut2}$, harboring R96, R103, and R105 substitutions to alanine or glutamate, respectively, remained dimeric in solution.

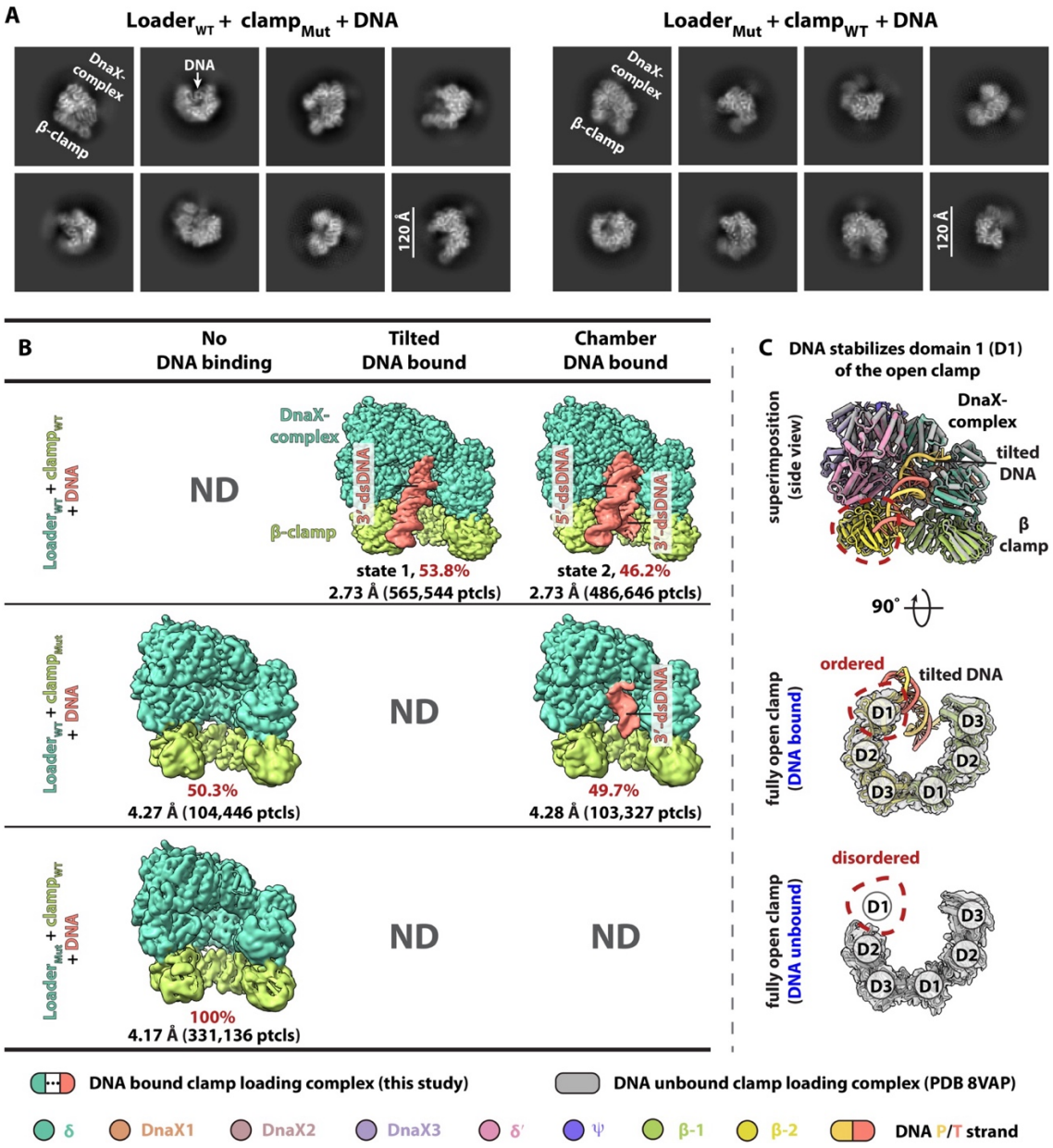

Figure S3. Cryo-EM analysis of the effects of mutations on β-clamp loading. (**A**) Representative 2D class averages of assembled clamp loading complexes containing mutant components. Left: wild-type DnaX-complex (loader$_{WT}$) assembled with a β-clamp basic patch mutant harboring R96A, R103A, and R105A substitutions (β-clamp$_{Mut}$) and 1-nt gapped DNA. Right: DnaX-complex bearing the δ-subunit Y316A substitution (loader$_{Mut}$) assembled with wild-type β-clamp (clamp$_{WT}$) and 1-nt gapped DNA. Assemblies were performed under same conditions as used for wild-type complexes. Key components and scale bar are indicated. (**B**) Reconstructed cryo-EM maps corresponding to the assemblies shown in (A**)**. For comparison, representative maps from wild-type clamp and clamp loader assemblies are also shown (state 1 conformer 1 and state 2 conformer 1). Total particle numbers for each state (summed across conformers) are listed to indicate relative populations. For assemblies containing wild-type clamp and loader, no clamp–clamp loader–only complex (lacking DNA) was observed. In contrast, assemblies

1096 containing β-clamp$_{Mut}$ yielded approximately equal populations of clamp–clamp loader–only complexes
1097 and complexes containing chamber-bound 3′-dsDNA, but no intermediates with tilted 3′-dsDNA or bent
1098 5′-were detected, consistent with the requirement for the β-clamp basic patch in DNA binding. For
1099 assemblies containing loader$_{Mut}$, only clamp–clamp loader–only complex was observed, with no DNA -
1100 bound state observed, indicating that the δ-subunit Y316 is critical for DNA recognition and subsequent
1101 clamp loading. ND, not detected. (**C**) DNA binding at the β-clamp basic patch stabilizes β-clamp domain
1102 I. Superimposition of structures of the DnaX-complex with an open β-clamp in the absence of DNA (gray,
1103 PDB: 8VAP)[17] and in the presence of 1-nt gapped DNA (colored; state 1 conformer 1 from this study) is
1104 showed. The clamp loader is omitted in the bottom views for clarity.
1105

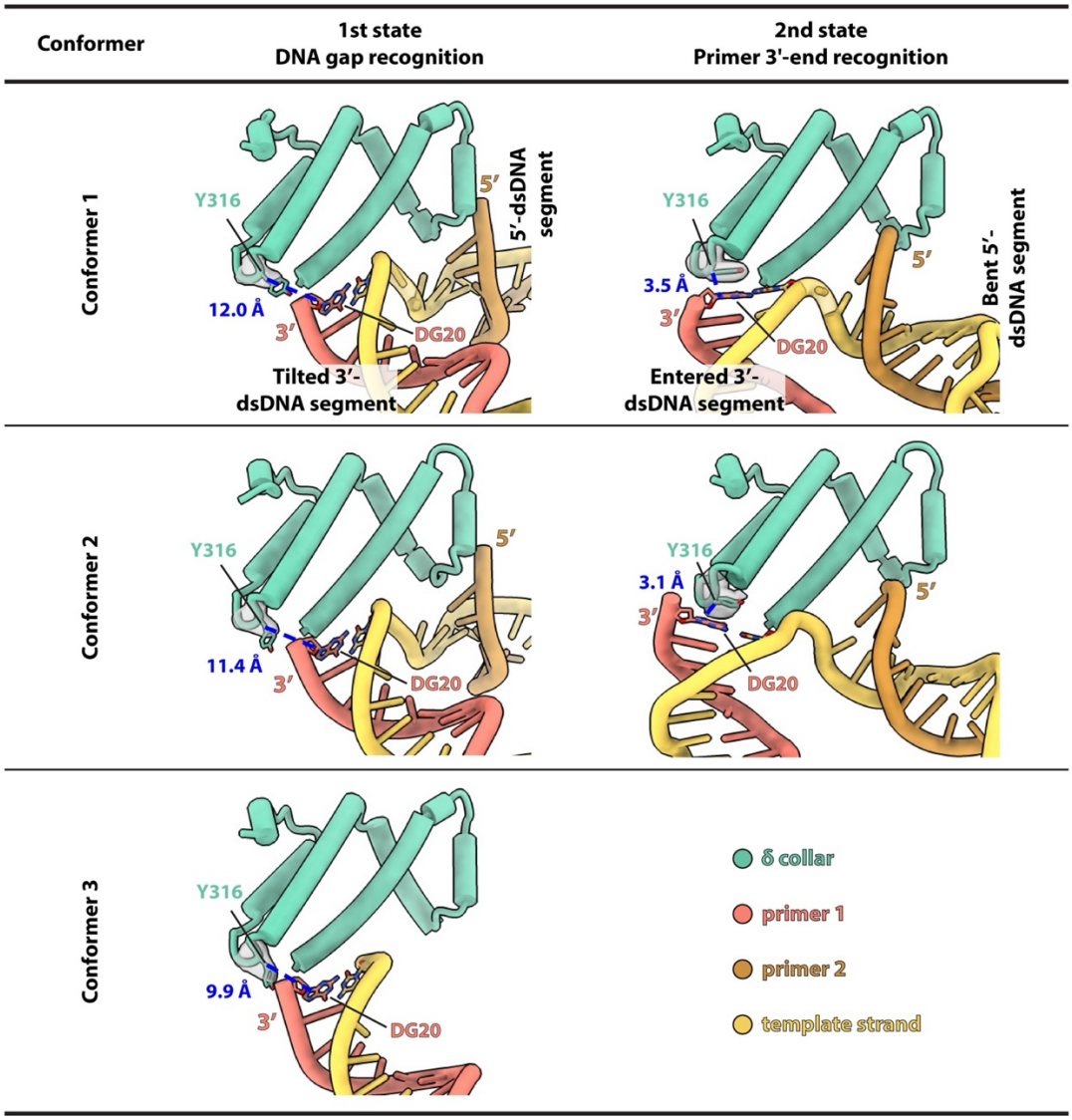

Figure S4. The *E. coli* clamp loader residue δ Y316 recognizes the recessed DNA 3′ end to facilitate proper positioning of the 3′-dsDNA within the loader chamber. In the first DNA gap recognition state, comparison of conformers 1–3 shows a progressive decrease in the distance between δ Y316 and the DNA 3′ end, from 12.0 Å to 9.9 Å, accompanied by increasingly well-defined local cryo-EM density for Y316. In the second state, corresponding to DNA primer 3′ end recognition, this distance is further reduced to ~3.3 Å in both conformers, and Y316 adopts a base-mimicking conformation that stacks against the terminal base G20 of the primer 3′ end, resulting in full stabilization of this residue. For clarity, only a closed-up view of this region is shown. Distance were measured between the Y316 Cβ atom and G20 C8 atom, which approximates the distance between the centers of the two ring-containing residues in the second state.

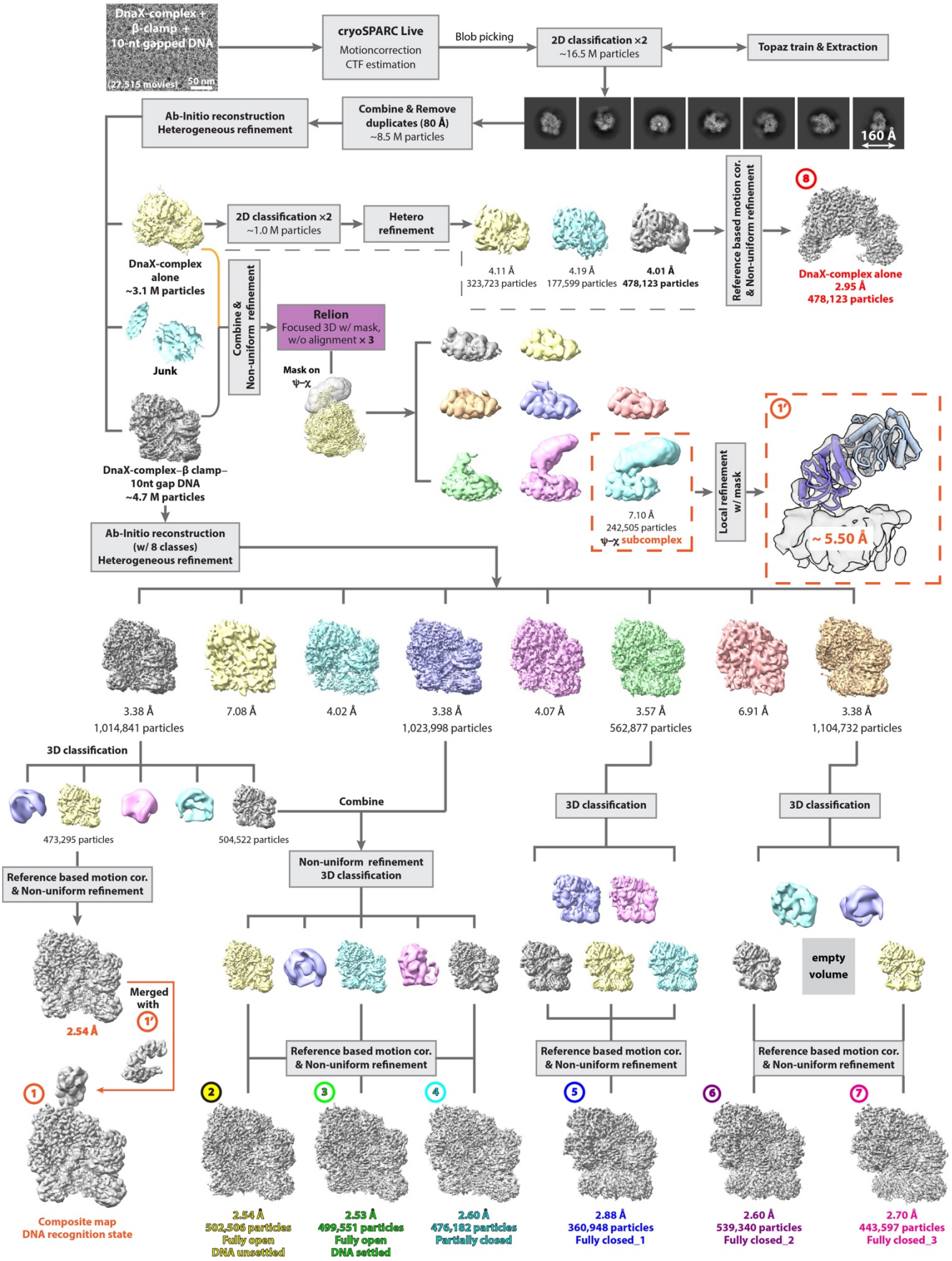
DnaX-complex + β-clamp + 10-nt gapped DNA
(27,515 movies)
50 nm
cryoSPARC Live
Motioncorrection
CTF estimation
Blob picking
2D classification ×2
~16.5 M particles
Topaz train & Extraction
160 Å
Combine & Remove duplicates (80 Å)
~8.5 M particles
Ab-Initio reconstruction
Heterogeneous refinement
DnaX-complex alone
~3.1 M particles
Junk
DnaX-complex–β clamp–10nt gap DNA
~4.7 M particles
2D classification ×2
~1.0 M particles
Hetero refinement
4.11 Å
323,723 particles
4.19 Å
177,599 particles
4.01 Å
478,123 particles
Reference based motion cor. & Non-uniform refinement
8
DnaX-complex alone
2.95 Å
478,123 particles
Combine & Non-uniform refinement
Relion
Focused 3D w/ mask, w/o alignment × 3
Mask on ψ–χ
7.10 Å
242,505 particles
ψ–χ subcomplex
Local refinement w/ mask
1'
~ 5.50 Å
Ab-Initio reconstruction (w/ 8 classes)
Heterogeneous refinement
3.38 Å
1,014,841 particles
7.08 Å
4.02 Å
3.38 Å
1,023,998 particles
4.07 Å
3.57 Å
562,877 particles
6.91 Å
3.38 Å
1,104,732 particles
3D classification
473,295 particles
504,522 particles
Combine
Reference based motion cor. & Non-uniform refinement
2.54 Å
Merged with
1'
1
Composite map
DNA recognition state
Non-uniform refinement
3D classification
Reference based motion cor. & Non-uniform refinement
2
2.54 Å
502,506 particles
Fully open
DNA unsettled
3
2.53 Å
499,551 particles
Fully open
DNA settled
4
2.60 Å
476,182 particles
Partially closed
3D classification
Reference based motion cor. & Non-uniform refinement
5
2.88 Å
360,948 particles
Fully closed_1
3D classification
empty volume
Reference based motion cor. & Non-uniform refinement
6
2.60 Å
539,340 particles
Fully closed_2
7
2.70 Å
443,597 particles
Fully closed_3

1121 **Figure S5. Cryo-EM data processing of the DnaX-complex–β-clamp bound to 10-nt gapped DNA.**
1122 A representative micrograph from ~28,000 movies collected on a 300kV Titan Krios microscope is
1123 shown, with scale bar indicated. Image processing was performed using cryoSPARC v4.5 and Relion
1124 v5.0[68,88]. Eight distinct clamp loading states were resolved at resolutions from ~3.0 Å to 2.5 Å, with
1125 density corresponding to the χψ heterodimer merged into the state 2 map. The χψ crystal structure
1126 bound to an SSB peptide bound (PDB: 3SXU) was rigid-body fitted into the locally refined 3D map
1127 highlighted by dashed red squares.
1128
1129

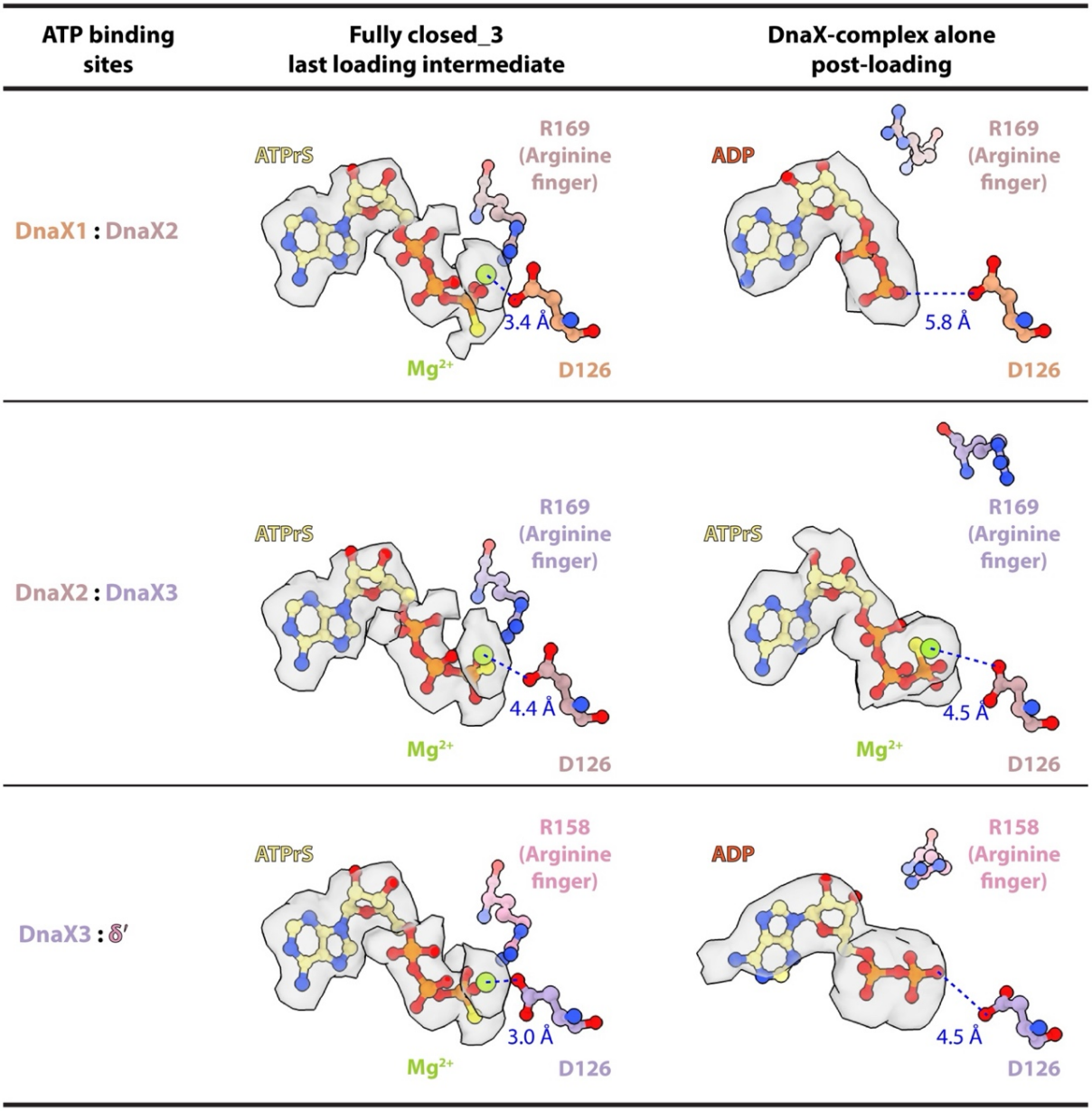

Figure S6. ATPγS hydrolysis is observed only in the DnaX-complex–alone structure. Across all 13 clamp loading intermediates captured with either 1-nt or 10-nt gapped DNA, ATPγS was bound to all ATPase sites from the fully open β-clamp state through the final fully closed state, indicating no ATPγS hydrolysis during these intermediates. The last loading intermediates (fully closed_3) is shown here as a representative example. In this state, the distances between the Mg^{2+} ion and the catalytic residue D126 (Walker B/DEAD box) are 3.4 Å and 3.0 Å at the first and third ATPase sites, respectively, consistent with a geometry competent for hydrolysis, whereas the distance at the second site is 4.4 Å. By contrast, in the DnaX-complex–alone structure, ADP can be unambiguously modeled at the first and third sites, while ATPγS remained bound at the second site, indicating that ATPγS hydrolysis had occurred at two sites following clamp loading. For clarity, only the bound nucleotides and key catalytic residues are shown.

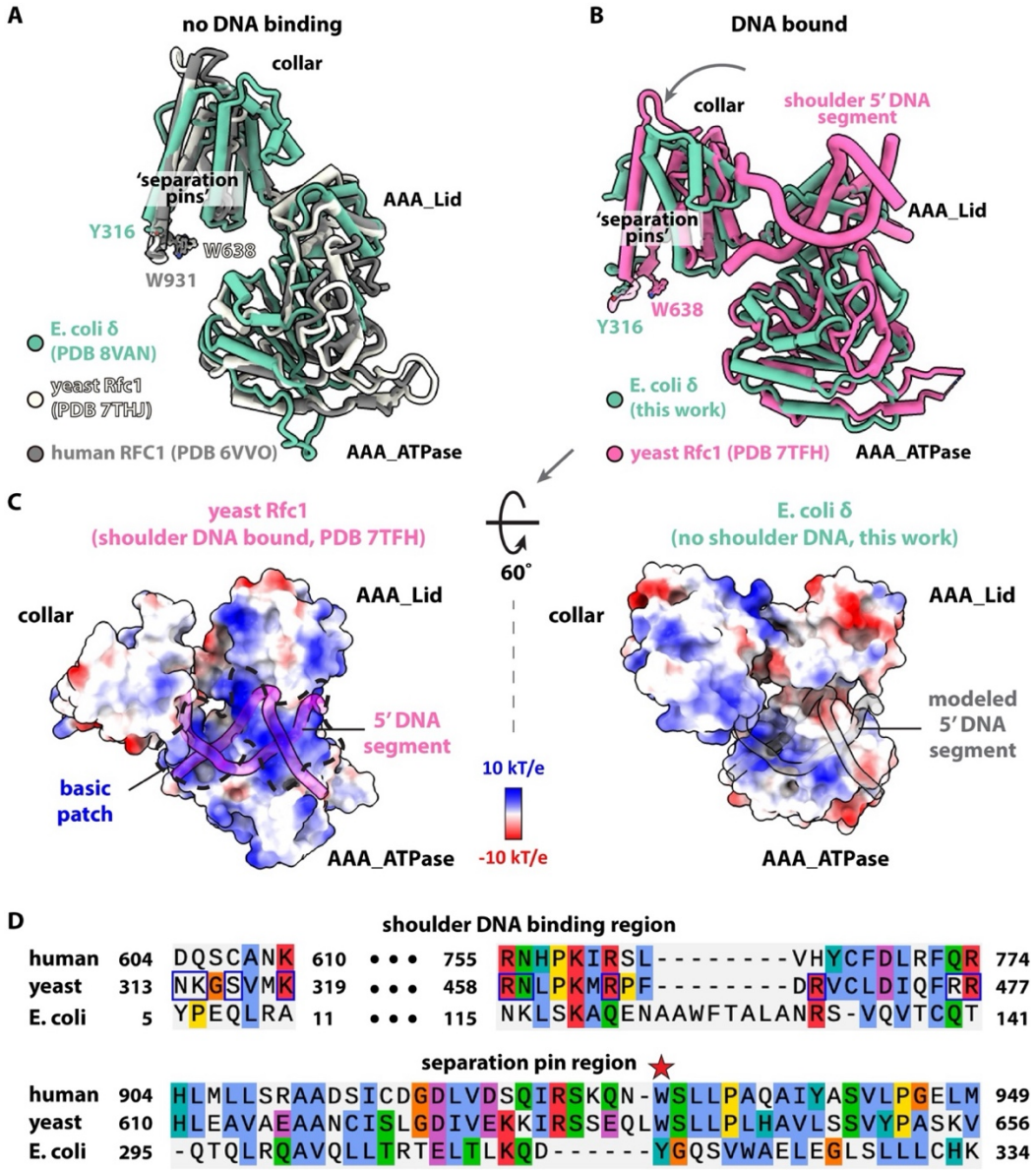

Figure S7. Comparisons of the clamp loader first subunit from *E. coli*, yeast, and human. (**A**) In the absence of DNA binding, the overall structures of *E. coli* δ, yeast Rfc1, and human RFC1 are similar. (**B**) Upon binding of the 3′-dsDNA in the chamber (omitted), the yeast Rfc1 AAA Lid and Collar domains undergo a larger movement than those in *E. coli*, creating additional space to facilitate subsequent binding of 5′-dsDNA at the shoulder. (**C**) The Rfc1 shoulder region presents a large basic patch (black dashed line) for 5′-dsDNA binding (left), which is absent in *E. coli* δ; steric clashes are observed when the Rfc1-bound 5′-dsDNA is modeled onto *E. coli* δ (right). (**D**) Structural-based sequence alignment shows that the shoulder regions of yeast Rfc1 and human RFC1 are more positively charged than that of *E. coli* δ (upper). The 'separation pin' in human and yeast proteins is a Trp residue with two aromatic rings, whereas the *E. coli* protein contains a Tyr residue with a single aromatic ring (lower). Residues are colored by chemical property (scheme from the MUSCLE alignment program[90]).

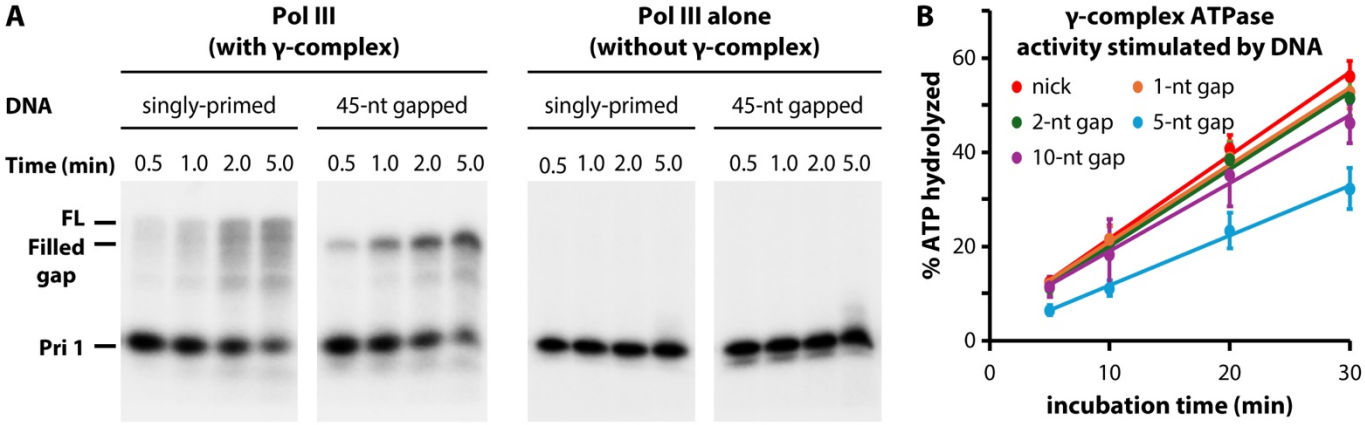

Figure S8. Characterization of Pol III DNA synthesis and DnaX-complex ATPase activity on distinct DNA substrates. (**A**) Urea–PAGE analysis of ^{32}P-labelled primer extension over increasing loading times using either singly primed or gapped DNA, in the presence (left) or absence (right) of the γ-complex. A sufficient amount of Pol III was added to saturate the reaction, making clamp loading the rate limiting step. (**B**) Stimulation of DnaX-complex ATPase activities by DNA substrates containing gaps of different sizes. See **Methods** for details.

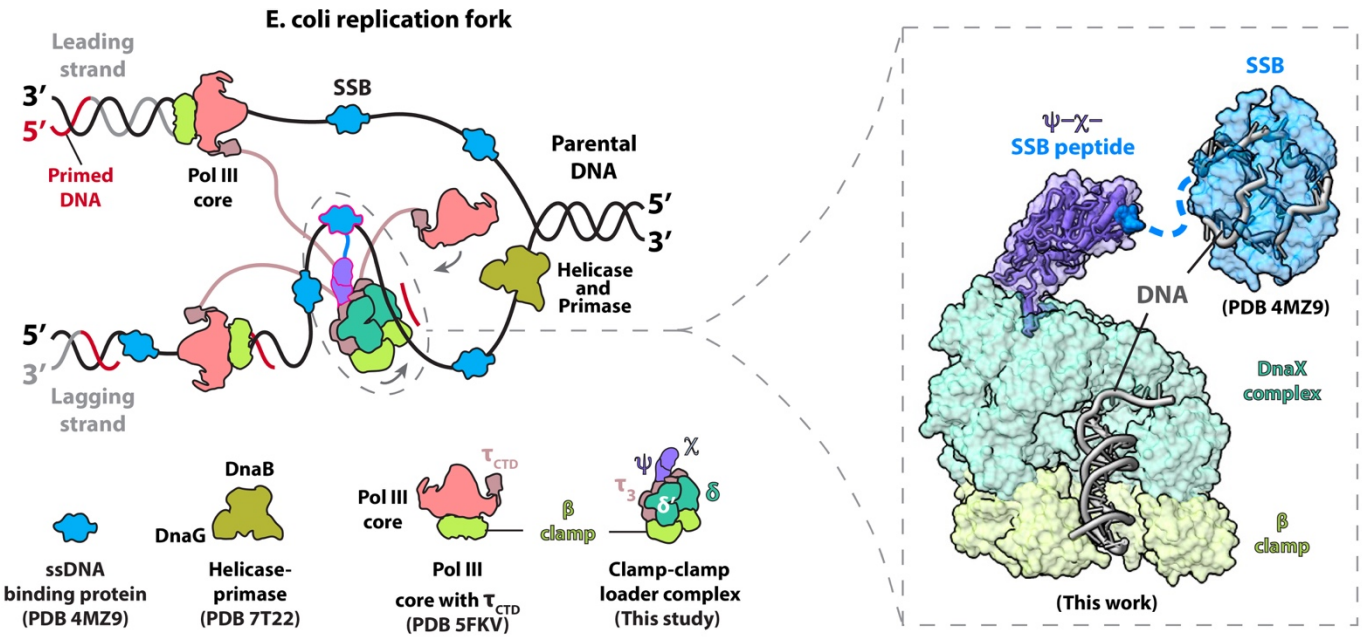

Figure S9. Model for coordination of the replisome by the DnaX-holo-complex. Left, a simplified model of the *E. coli* replication fork is shown, including the DnaB helicase encircling the lagging strand and unwinding parental DNA, the DnaG primase bound to DnaB and synthesizing RNA primers on the lagging strand template, and multiple SSB molecules coating the ssDNA. In addition to loading the β-clamp for Pol III on both the leading and lagging strands, the DnaX-holo-complex organizes the replication fork by interacting with SSB via its χ subunit and with three Pol III molecules via the C-terminal domains of its three τ subunits (τ_{CTD})[61,62]. These interactions may facilitate recruitment of Pol III to the loaded β-clamp. Key components are listed together with the available PDB codes. Right, a structural model shows SSB bound to ssDNA and interacting with the DnaX-holo-complex through its flexibly linked C-terminal peptide (blue surface).

REFERENCES

1. Stukenberg, P.T., Studwell-Vaughan, P.S., and O'Donnell, M. (1991). Mechanism of the sliding beta-clamp of DNA polymerase III holoenzyme. The Journal of biological chemistry *266*, 11328-11334.
2. Kong, X.P., Onrust, R., O'Donnell, M., and Kuriyan, J. (1992). Three-dimensional structure of the beta subunit of E. coli DNA polymerase III holoenzyme: a sliding DNA clamp. Cell *69*, 425-437. 10.1016/0092-8674(92)90445-i.
3. Kelch, B.A., Makino, D.L., O'Donnell, M., and Kuriyan, J. (2012). Clamp loader ATPases and the evolution of DNA replication machinery. BMC Biol *10*, 34. 10.1186/1741-7007-10-34.
4. O'Donnell, M., Langston, L., and Stillman, B. (2013). Principles and concepts of DNA replication in bacteria, archaea, and eukarya. Cold Spring Harb Perspect Biol *5*. 10.1101/cshperspect.a010108.
5. Krishna, T.S., Kong, X.P., Gary, S., Burgers, P.M., and Kuriyan, J. (1994). Crystal structure of the eukaryotic DNA polymerase processivity factor PCNA. Cell *79*, 1233-1243. 10.1016/0092-8674(94)90014-0.
6. Gulbis, J.M., Kelman, Z., Hurwitz, J., O'Donnell, M., and Kuriyan, J. (1996). Structure of the C-terminal region of p21(WAF1/CIP1) complexed with human PCNA. Cell *87*, 297-306. 10.1016/s0092-8674(00)81347-1.
7. Jeruzalmi, D., O'Donnell, M., and Kuriyan, J. (2001). Crystal structure of the processivity clamp loader gamma (gamma) complex of E. coli DNA polymerase III. Cell *106*, 429-441. 10.1016/s0092-8674(01)00463-9.
8. Johnson, A., and O'Donnell, M. (2005). Cellular DNA replicases: components and dynamics at the replication fork. Annu Rev Biochem *74*, 283-315. 10.1146/annurev.biochem.73.011303.073859.
9. Ellison, V., and Stillman, B. (1998). Reconstitution of recombinant human replication factor C (RFC) and identification of an RFC subcomplex possessing DNA-dependent ATPase activity. The Journal of biological chemistry *273*, 5979-5987. 10.1074/jbc.273.10.5979.
10. Bowman, G.D., O'Donnell, M., and Kuriyan, J. (2004). Structural analysis of a eukaryotic sliding DNA clamp-clamp loader complex. Nature *429*, 724-730. 10.1038/nature02585.
11. Kelch, B., Makino, D., Simonetta, K., O'Donnell, M., and Kuriyan, J. (2012). Molecular Mechanisms of DNA Polymerase Clamp Loaders. Macromolecular Crystallography, 103-114.
12. Gaubitz, C., Liu, X., Pajak, J., Stone, N.P., Hayes, J.A., Demo, G., and Kelch, B.A. (2022). Cryo-EM structures reveal high-resolution mechanism of a DNA polymerase sliding clamp loader. Elife *11*. 10.7554/eLife.74175.
13. Zheng, F., Georgescu, R., Yao, N.Y., Li, H., and O'Donnell, M.E. (2022). Cryo-EM structures reveal that RFC recognizes both the 3'- and 5'-DNA ends to load PCNA onto gaps for DNA repair. Elife *11*. 10.7554/eLife.77469.
14. Liu, X., Gaubitz, C., Pajak, J., and Kelch, B.A. (2022). A second DNA binding site on RFC facilitates clamp loading at gapped or nicked DNA. Elife *11*. 10.7554/eLife.77483.
15. Schrecker, M., Castaneda, J.C., Devbhandari, S., Kumar, C., Remus, D., and Hite, R.K. (2022). Multistep loading of a DNA sliding clamp onto DNA by replication factor C. Elife *11*. 10.7554/eLife.78253.
16. Xu, Z.Q., Jergic, S., Lo, A.T.Y., Pradhan, A.C., Brown, S.H.J., Bouwer, J.C., Ghodke, H., Lewis, P.J., Tolun, G., Oakley, A.J., and Dixon, N.E. (2024). Structural characterisation of the complete cycle of sliding clamp loading in Escherichia coli. Nat Commun *15*, 8372. 10.1038/s41467-024-52623-9.
17. Landeck, J.T., Pajak, J., Norman, E.K., Sedivy, E.L., and Kelch, B.A. (2024). Differences between bacteria and eukaryotes in clamp loader mechanism, a conserved process underlying DNA replication. The Journal of biological chemistry *300*, 107166. 10.1016/j.jbc.2024.107166.
18. Turner, J., Hingorani, M.M., Kelman, Z., and O'Donnell, M. (1999). The internal workings of a DNA polymerase clamp-loading machine. EMBO J *18*, 771-783. 10.1093/emboj/18.3.771.

1230 19. Johnson, A., and O'Donnell, M. (2003). Ordered ATP hydrolysis in the gamma complex clamp
1231 loader AAA+ machine. The Journal of biological chemistry *278*, 14406-14413.
1232 10.1074/jbc.M212708200.
1233 20. Johnson, A., Yao, N.Y., Bowman, G.D., Kuriyan, J., and O'Donnell, M. (2006). The replication
1234 factor C clamp loader requires arginine finger sensors to drive DNA binding and proliferating cell
1235 nuclear antigen loading. The Journal of biological chemistry *281*, 35531-35543.
1236 10.1074/jbc.M606090200.
1237 21. Li, H., O'Donnell, M., and Kelch, B. (2022). Unexpected new insights into DNA clamp loaders:
1238 Eukaryotic clamp loaders contain a second DNA site for recessed 5' ends that facilitates repair
1239 and signals DNA damage: Eukaryotic clamp loaders contain a second DNA site for recessed 5'
1240 ends that facilitates repair and signals DNA damage. Bioessays *44*, e2200154.
1241 10.1002/bies.202200154.
1242 22. Liu, J., Zhou, Y., and Hingorani, M.M. (2017). Linchpin DNA-binding residues serve as go/no-go
1243 controls in the replication factor C-catalyzed clamp-loading mechanism. The Journal of biological
1244 chemistry *292*, 15892-15906. 10.1074/jbc.M117.798702.
1245 23. Marzahn, M.R., Hayner, J.N., Meyer, J.A., and Bloom, L.B. (2015). Kinetic analysis of PCNA
1246 clamp binding and release in the clamp loading reaction catalyzed by Saccharomyces cerevisiae
1247 replication factor C. Biochim Biophys Acta *1854*, 31-38. 10.1016/j.bbapap.2014.09.019.
1248 24. Sakato, M., Zhou, Y., and Hingorani, M.M. (2012). ATP binding and hydrolysis-driven rate-
1249 determining events in the RFC-catalyzed PCNA clamp loading reaction. J Mol Biol *416*, 176-191.
1250 10.1016/j.jmb.2011.12.018.
1251 25. Zheng, F., Georgescu, R.E., Yao, N.Y., O'Donnell, M.E., and Li, H. (2022). DNA is loaded
1252 through the 9-1-1 DNA checkpoint clamp in the opposite direction of the PCNA clamp. Nat Struct
1253 Mol Biol *29*, 376-385. 10.1038/s41594-022-00742-6.
1254 26. Castaneda, J.C., Schrecker, M., Remus, D., and Hite, R.K. (2022). Mechanisms of loading and
1255 release of the 9-1-1 checkpoint clamp. Nat Struct Mol Biol *29*, 369-375. 10.1038/s41594-022-
1256 00741-7.
1257 27. Day, M., Oliver, A.W., and Pearl, L.H. (2022). Structure of the human RAD17-RFC clamp loader
1258 and 9-1-1 checkpoint clamp bound to a dsDNA-ssDNA junction. Nucleic Acids Res *50*, 8279-
1259 8289. 10.1093/nar/gkac588.
1260 28. Simonetta, K.R., Kazmirski, S.L., Goedken, E.R., Cantor, A.J., Kelch, B.A., McNally, R., Seyedin,
1261 S.N., Makino, D.L., O'Donnell, M., and Kuriyan, J. (2009). The mechanism of ATP-dependent
1262 primer-template recognition by a clamp loader complex. Cell *137*, 659-671.
1263 10.1016/j.cell.2009.03.044.
1264 29. Onrust, R., Finkelstein, J., Naktinis, V., Turner, J., Fang, L., and O'Donnell, M. (1995). Assembly
1265 of a chromosomal replication machine: two DNA polymerases, a clamp loader, and sliding clamps
1266 in one holoenzyme particle. I. Organization of the clamp loader. The Journal of biological
1267 chemistry *270*, 13348-13357. 10.1074/jbc.270.22.13348.
1268 30. Yao, N., Turner, J., Kelman, Z., Stukenberg, P.T., Dean, F., Shechter, D., Pan, Z.Q., Hurwitz, J.,
1269 and O'Donnell, M. (1996). Clamp loading, unloading and intrinsic stability of the PCNA, beta and
1270 gp45 sliding clamps of human, E. coli and T4 replicases. Genes Cells *1*, 101-113.
1271 10.1046/j.1365-2443.1996.07007.x.
1272 31. Zheng, F., Georgescu, R.E., Yao, N.Y., O'Donnell, M.E., and Li, H. (2023). Structures of 9-1-1
1273 DNA checkpoint clamp loading at gaps from start to finish and ramification on biology. Cell Rep
1274 *42*, 112694. 10.1016/j.celrep.2023.112694.
1275 32. Yao, N., Leu, F.P., Anjelkovic, J., Turner, J., and O'Donnell, M. (2000). DNA structure
1276 requirements for the Escherichia coli gamma complex clamp loader and DNA polymerase III
1277 holoenzyme. The Journal of biological chemistry *275*, 11440-11450. 10.1074/jbc.275.15.11440.
1278 33. Ason, B., Handayani, R., Williams, C.R., Bertram, J.G., Hingorani, M.M., O'Donnell, M.,
1279 Goodman, M.F., and Bloom, L.B. (2003). Mechanism of loading the Escherichia coli DNA
1280 polymerase III beta sliding clamp on DNA. Bona fide primer/templates preferentially trigger the
1281 gamma complex to hydrolyze ATP and load the clamp. The Journal of biological chemistry *278*,
1282 10033-10040. 10.1074/jbc.M211741200.

1283 34. Snyder, A.K., Williams, C.R., Johnson, A., O'Donnell, M., and Bloom, L.B. (2004). Mechanism of
1284 loading the Escherichia coli DNA polymerase III sliding clamp: II. Uncoupling the beta and DNA
1285 binding activities of the gamma complex. The Journal of biological chemistry *279*, 4386-4393.
1286 10.1074/jbc.M310430200.
1287 35. Gaubitz, C., Liu, X., Magrino, J., Stone, N.P., Landeck, J., Hedglin, M., and Kelch, B.A. (2020).
1288 Structure of the human clamp loader reveals an autoinhibited conformation of a substrate-bound
1289 AAA+ switch. Proc Natl Acad Sci U S A *117*, 23571-23580. 10.1073/pnas.2007437117.
1290 36. Marceau, A.H., Bahng, S., Massoni, S.C., George, N.P., Sandler, S.J., Marians, K.J., and Keck,
1291 J.L. (2011). Structure of the SSB-DNA polymerase III interface and its role in DNA replication.
1292 EMBO J *30*, 4236-4247. 10.1038/emboj.2011.305.
1293 37. Tondnevis, F., Gillilan, R.E., Bloom, L.B., and McKenna, R. (2015). Solution study of the
1294 Escherichia coli DNA polymerase III clamp loader reveals the location of the dynamic psichi
1295 heterodimer. Struct Dyn *2*, 054701. 10.1063/1.4927407.
1296 38. Gomes, X.V., Gary, S.L., and Burgers, P.M. (2000). Overproduction in Escherichia coli and
1297 characterization of yeast replication factor C lacking the ligase homology domain. The Journal of
1298 biological chemistry *275*, 14541-14549. 10.1074/jbc.275.19.14541.
1299 39. Rajagopalan, M., Lu, C., Woodgate, R., O'Donnell, M., Goodman, M.F., and Echols, H. (1992).
1300 Activity of the purified mutagenesis proteins UmuC, UmuD', and RecA in replicative bypass of an
1301 abasic DNA lesion by DNA polymerase III. Proc Natl Acad Sci U S A *89*, 10777-10781.
1302 10.1073/pnas.89.22.10777.
1303 40. Indiani, C., Langston, L.D., Yurieva, O., Goodman, M.F., and O'Donnell, M. (2009). Translesion
1304 DNA polymerases remodel the replisome and alter the speed of the replicative helicase. Proc
1305 Natl Acad Sci U S A *106*, 6031-6038. 10.1073/pnas.0901403106.
1306 41. Indiani, C., McInerney, P., Georgescu, R., Goodman, M.F., and O'Donnell, M. (2005). A sliding-
1307 clamp toolbelt binds high- and low-fidelity DNA polymerases simultaneously. Mol Cell *19*, 805-
1308 815. 10.1016/j.molcel.2005.08.011.
1309 42. Indiani, C., Patel, M., Goodman, M.F., and O'Donnell, M.E. (2013). RecA acts as a switch to
1310 regulate polymerase occupancy in a moving replication fork. Proc Natl Acad Sci U S A *110*, 5410-
1311 5415. 10.1073/pnas.1303301110.
1312 43. Bonner, C.A., Stukenberg, P.T., Rajagopalan, M., Eritja, R., O'Donnell, M., McEntee, K., Echols,
1313 H., and Goodman, M.F. (1992). Processive DNA synthesis by DNA polymerase II mediated by
1314 DNA polymerase III accessory proteins. The Journal of biological chemistry *267*, 11431-11438.
1315 44. Wagner, J., Fujii, S., Gruz, P., Nohmi, T., and Fuchs, R.P. (2000). The beta clamp targets DNA
1316 polymerase IV to DNA and strongly increases its processivity. EMBO Rep *1*, 484-488.
1317 10.1093/embo-reports/kvd109.
1318 45. Bloom, L.B. (2009). Loading clamps for DNA replication and repair. DNA Repair (Amst) *8*, 570-
1319 578. 10.1016/j.dnarep.2008.12.014.
1320 46. Lopez de Saro, F.J., and O'Donnell, M. (2001). Interaction of the beta sliding clamp with MutS,
1321 ligase, and DNA polymerase I. Proc Natl Acad Sci U S A *98*, 8376-8380.
1322 10.1073/pnas.121009498.
1323 47. Becherel, O.J., Fuchs, R.P., and Wagner, J. (2002). Pivotal role of the beta-clamp in translesion
1324 DNA synthesis and mutagenesis in E. coli cells. DNA Repair (Amst) *1*, 703-708. 10.1016/s1568-
1325 7864(02)00106-4.
1326 48. Yang, W. (2003). Damage repair DNA polymerases Y. Curr Opin Struct Biol *13*, 23-30.
1327 10.1016/s0959-440x(02)00003-9.
1328 49. Maul, R.W., Ponticelli, S.K., Duzen, J.M., and Sutton, M.D. (2007). Differential binding of
1329 Escherichia coli DNA polymerases to the beta-sliding clamp. Mol Microbiol *65*, 811-827.
1330 10.1111/j.1365-2958.2007.05828.x.
1331 50. Kath, J.E., Chang, S., Scotland, M.K., Wilbertz, J.H., Jergic, S., Dixon, N.E., Sutton, M.D., and
1332 Loparo, J.J. (2016). Exchange between Escherichia coli polymerases II and III on a processivity
1333 clamp. Nucleic Acids Res *44*, 1681-1690. 10.1093/nar/gkv1375.
1334 51. Furukohri, A., Goodman, M.F., and Maki, H. (2008). A dynamic polymerase exchange with
1335 Escherichia coli DNA polymerase IV replacing DNA polymerase III on the sliding clamp. The
1336 Journal of biological chemistry *283*, 11260-11269. 10.1074/jbc.M709689200.

52. Kath, J.E., Jergic, S., Heltzel, J.M., Jacob, D.T., Dixon, N.E., Sutton, M.D., Walker, G.C., and Loparo, J.J. (2014). Polymerase exchange on single DNA molecules reveals processivity clamp control of translesion synthesis. Proc Natl Acad Sci U S A *111*, 7647-7652. 10.1073/pnas.1321076111.
53. Fijalkowska, I.J., Schaaper, R.M., and Jonczyk, P. (2012). DNA replication fidelity in Escherichia coli: a multi-DNA polymerase affair. FEMS Microbiol Rev *36*, 1105-1121. 10.1111/j.1574-6976.2012.00338.x.
54. Li, N., Lam, W.H., Zhai, Y., Cheng, J., Cheng, E., Zhao, Y., Gao, N., and Tye, B.K. (2018). Structure of the origin recognition complex bound to DNA replication origin. Nature *559*, 217-222. 10.1038/s41586-018-0293-x.
55. Correction for Yuan et al., Structural mechanism of helicase loading onto replication origin DNA by ORC-Cdc6. (2021). Proc Natl Acad Sci U S A *118*. 10.1073/pnas.2025413118.
56. Neylon, C., Kralicek, A.V., Hill, T.M., and Dixon, N.E. (2005). Replication termination in Escherichia coli: structure and antihelicase activity of the Tus-Ter complex. Microbiol Mol Biol Rev *69*, 501-526. 10.1128/MMBR.69.3.501-526.2005.
57. Simonsen, S., Sogaard, C.K., Olsen, J.G., Otterlei, M., and Kragelund, B.B. (2024). The bacterial DNA sliding clamp, beta-clamp: structure, interactions, dynamics and drug discovery. Cell Mol Life Sci *81*, 245. 10.1007/s00018-024-05252-w.
58. Moolman, M.C., Krishnan, S.T., Kerssemakers, J.W., van den Berg, A., Tulinski, P., Depken, M., Reyes-Lamothe, R., Sherratt, D.J., and Dekker, N.H. (2014). Slow unloading leads to DNA-bound beta2-sliding clamp accumulation in live Escherichia coli cells. Nat Commun *5*, 5820. 10.1038/ncomms6820.
59. Lazowski, K., Woodgate, R., and Fijalkowska, I.J. (2024). Escherichia coli DNA replication: the old model organism still holds many surprises. FEMS Microbiol Rev *48*. 10.1093/femsre/fuae018.
60. Fernandez-Leiro, R., Conrad, J., Scheres, S.H.W., and Lamers, M.H. (2015). cryo-EM structures of the E. coli replicative DNA polymerase reveal its dynamic interactions with the DNA sliding clamp, exonuclease and τ. eLife *4*, e11134. 10.7554/eLife.11134.
61. Reyes-Lamothe, R., Sherratt, D.J., and Leake, M.C. (2010). Stoichiometry and architecture of active DNA replication machinery in Escherichia coli. Science *328*, 498-501. 10.1126/science.1185757.
62. McInerney, P., Johnson, A., Katz, F., and O'Donnell, M. (2007). Characterization of a triple DNA polymerase replisome. Mol Cell *27*, 527-538. 10.1016/j.molcel.2007.06.019.
63. Kelman, Z., Yuzhakov, A., Andjelkovic, J., and O'Donnell, M. (1998). Devoted to the lagging strand-the subunit of DNA polymerase III holoenzyme contacts SSB to promote processive elongation and sliding clamp assembly. EMBO J *17*, 2436-2449. 10.1093/emboj/17.8.2436.
64. Kelman, Z., Yao, N., and O'Donnell, M. (1995). Escherichia coli expression vectors containing a protein kinase recognition motif, His6-tag and hemagglutinin epitope. Gene *166*, 177-178. 10.1016/0378-1119(95)00556-7.
65. Studwell, P.S., and O'Donnell, M. (1990). Processive replication is contingent on the exonuclease subunit of DNA polymerase III holoenzyme. The Journal of biological chemistry *265*, 1171-1178.
66. Kelman, Z., Naktinis, V., and O'Donnell, M. (1995). Radiolabeling of proteins for biochemical studies. Methods Enzymol *262*, 430-442. 10.1016/0076-6879(95)62034-6.
67. Mastronarde, D.N. (2003). SerialEM: A Program for Automated Tilt Series Acquisition on Tecnai Microscopes Using Prediction of Specimen Position. Microscopy and Microanalysis *9*, 1182 - 1183.
68. Punjani, A., Rubinstein, J.L., Fleet, D.J., and Brubaker, M.A. (2017). cryoSPARC: algorithms for rapid unsupervised cryo-EM structure determination. Nat Methods *14*, 290-296. 10.1038/nmeth.4169.
69. Scheres, S.H. (2012). RELION: implementation of a Bayesian approach to cryo-EM structure determination. J Struct Biol *180*, 519-530. 10.1016/j.jsb.2012.09.006.
70. Zheng, S.Q., Palovcak, E., Armache, J.P., Verba, K.A., Cheng, Y., and Agard, D.A. (2017). MotionCor2: anisotropic correction of beam-induced motion for improved cryo-electron microscopy. Nat Methods *14*, 331-332. 10.1038/nmeth.4193.

71. Rohou, A., and Grigorieff, N. (2015). CTFFIND4: Fast and accurate defocus estimation from electron micrographs. J Struct Biol *192*, 216-221. 10.1016/j.jsb.2015.08.008.
72. Bepler, T., Morin, A., Rapp, M., Brasch, J., Shapiro, L., Noble, A.J., and Berger, B. (2019). Positive-unlabeled convolutional neural networks for particle picking in cryo-electron micrographs. Nat Methods *16*, 1153-1160. 10.1038/s41592-019-0575-8.
73. Asarnow, D., Palovcak, E., and Cheng, Y. (2019). UCSF pyem v0. 5. Zenodo https://doi. org/10.5281/zenodo *3576630*.
74. Pettersen, E.F., Goddard, T.D., Huang, C.C., Couch, G.S., Greenblatt, D.M., Meng, E.C., and Ferrin, T.E. (2004). UCSF Chimera--a visualization system for exploratory research and analysis. J Comput Chem *25*, 1605-1612. 10.1002/jcc.20084.
75. Goddard, T.D., Huang, C.C., Meng, E.C., Pettersen, E.F., Couch, G.S., Morris, J.H., and Ferrin, T.E. (2018). UCSF ChimeraX: Meeting modern challenges in visualization and analysis. Protein Sci *27*, 14-25. 10.1002/pro.3235.
76. Emsley, P., Lohkamp, B., Scott, W.G., and Cowtan, K. (2010). Features and development of Coot. Acta Crystallogr D Biol Crystallogr *66*, 486-501. 10.1107/S0907444910007493.
77. Adams, P.D., Afonine, P.V., Bunkoczi, G., Chen, V.B., Davis, I.W., Echols, N., Headd, J.J., Hung, L.W., Kapral, G.J., Grosse-Kunstleve, R.W., et al. (2010). PHENIX: a comprehensive Python-based system for macromolecular structure solution. Acta Crystallogr D Biol Crystallogr *66*, 213-221. 10.1107/S0907444909052925.
78. Zheng, F., Georgescu, R.E., Li, H., and O'Donnell, M.E. (2020). Structure of eukaryotic DNA polymerase delta bound to the PCNA clamp while encircling DNA. Proc Natl Acad Sci U S A *117*, 30344-30353. 10.1073/pnas.2017637117.
79. Sanchez-Garcia, R., Gomez-Blanco, J., Cuervo, A., Carazo, J.M., Sorzano, C.O.S., and Vargas, J. (2021). DeepEMhancer: a deep learning solution for cryo-EM volume post-processing. Commun Biol *4*, 874. 10.1038/s42003-021-02399-1.
80. He, J., Li, T., and Huang, S.Y. (2023). Improvement of cryo-EM maps by simultaneous local and non-local deep learning. Nat Commun *14*, 3217. 10.1038/s41467-023-39031-1.
81. Schwab, J., Kimanius, D., Burt, A., Dendooven, T., and Scheres, S.H.W. (2024). DynaMight: estimating molecular motions with improved reconstruction from cryo-EM images. Nat Methods *21*, 1855-1862. 10.1038/s41592-024-02377-5.
82. Asarnow, D., Palovcak, E., and Cheng, Y. (2019). UCSF pyem v0. 5. Zenodo *3576630*. https://doi.org/10.5281/zenodo.3576630.
83. Georgescu, R.E., Kim, S.-S., Yurieva, O., Kuriyan, J., Kong, X.-P., and O'Donnell, M. (2008). Structure of a Sliding Clamp on DNA. Cell *132*, 43-54. https://doi.org/10.1016/j.cell.2007.11.045.
84. Jamali, K., Kall, L., Zhang, R., Brown, A., Kimanius, D., and Scheres, S.H.W. (2024). Automated model building and protein identification in cryo-EM maps. Nature *628*, 450-457. 10.1038/s41586-024-07215-4.
85. Chen, V.B., Arendall, W.B., 3rd, Headd, J.J., Keedy, D.A., Immormino, R.M., Kapral, G.J., Murray, L.W., Richardson, J.S., and Richardson, D.C. (2010). MolProbity: all-atom structure validation for macromolecular crystallography. Acta Crystallogr D Biol Crystallogr *66*, 12-21. 10.1107/S0907444909042073.
86. Pettersen, E.F., Goddard, T.D., Huang, C.C., Meng, E.C., Couch, G.S., Croll, T.I., Morris, J.H., and Ferrin, T.E. (2021). UCSF ChimeraX: Structure visualization for researchers, educators, and developers. Protein Sci *30*, 70-82. 10.1002/pro.3943.
87. Oakley, A.J., Prosselkov, P., Wijffels, G., Beck, J.L., Wilce, M.C., and Dixon, N.E. (2003). Flexibility revealed by the 1.85 A crystal structure of the beta sliding-clamp subunit of Escherichia coli DNA polymerase III. Acta Crystallogr D Biol Crystallogr *59*, 1192-1199. 10.1107/s0907444903009958.
88. Kimanius, D., Jamali, K., Wilkinson, M.E., Lövestam, S., Velazhahan, V., Nakane, T., and Scheres, S.H.W. (2023). Data-driven regularisation lowers the size barrier of cryo-EM structure determination. bioRxiv, 2023.2010.2023.563586. 10.1101/2023.10.23.563586.
89. Stewart, J., Hingorani, M.M., Kelman, Z., and O'Donnell, M. (2001). Mechanism of beta clamp opening by the delta subunit of Escherichia coli DNA polymerase III holoenzyme. The Journal of biological chemistry *276*, 19182-19189. 10.1074/jbc.M100592200.

1444 90. Edgar, R.C. (2004). MUSCLE: multiple sequence alignment with high accuracy and high
1445 throughput. Nucleic Acids Res *32*, 1792-1797. 10.1093/nar/gkh340.
1446